NASA Technical Paper 1685

Wind-Tunnel Experiments on Divergence of Forward-Swept Wings

Rodney H. Ricketts and Robert V. Doggett, Jr.

AUGUST 1980

NASA

NASA Technical Paper 1685

Wind-Tunnel Experiments on Divergence of Forward-Swept Wings

Rodney H. Ricketts and Robert V. Doggett, Jr.
Langley Research Center
Hampton, Virginia

National Aeronautics
and Space Administration

**Scientific and Technical
Information Branch**

1980

SUMMARY

An experimental study to investigate the aeroelastic behavior of forward-swept wings was conducted in the Langley Transonic Dynamics Tunnel. Seven flat-plate models with varying aspect ratios and wing sweep angles were tested at low speeds in air. Three models having the same planform but different airfoil sections (flat-plate, conventional, and supercritical) were tested at transonic speeds in Freon[1] 12. Linear analyses were performed to provide predictions to compare with the measured aeroelastic instabilities, which include both static divergence and flutter. Six subcritical response testing techniques were formulated and evaluated at transonic speeds for accuracy in predicting static divergence. Two "divergence stoppers" were developed and evaluated for use in protecting the model from structural damage during tests.

INTRODUCTION

Forward-swept wing designs appear to offer selected aerodynamic performance improvements over conventional aft-swept wings, such as higher lift-drag ratios, lower trim drag, and better stall/spin characteristics (ref. 1). In addition, these designs may allow for improved fuselage-volume arrangements, by having the wing box located more rearward. Two powered, forward-swept wing aircraft, both of German design, are known to have been built to take advantage of these improvements. These aircraft include the World War II vintage Junkers Ju 287 (ref. 2) and a 1960's business jet (ref. 3). Until recently, serious consideration has not been given to forward-swept wing designs because forward sweep has led to an unfavorable static aeroelastic characteristic, namely, static divergence (in this paper, referred to simply as divergence). Potential gains in aerodynamic performance were more than offset by the increase in structural mass required to provide sufficient stiffness to insure adequate divergence speed margins. In the early 1970's, however, developments in composite structures technology appeared to offer a solution to the problem of structural mass increases required in the design of forward-swept wings. Analytical studies by Krone (ref. 4) showed that divergence speeds for forward-swept wings of composite materials can be increased substantially by optimally tailoring (arranging) the composite lamina thicknesses and orientations without incurring significant increases in structural mass above a so-called "strength design." As a consequence of these studies, interest was aroused in applying composite materials to forward-swept wings, particularly for fighter airplanes. The Defense Advanced Research Projects Agency (DARPA) in cooperation with the U.S. Air Force and the National Aeronautics and Space Administration (NASA) initiated a comprehensive analytical and experimental program to demonstrate the feasibility of using composite materials on advanced high-performance aircraft with forward-swept wings (ref. 1).

---

[1]Freon: Registered trademark of E. I. du Pont de Nemours & Co., Inc.

The objectives of the present study are (1) to provide some basic experimental data and analytical comparisons to aid in understanding divergence characteristics of forward-swept wings; and (2) to develop wind-tunnel experimental procedures applicable to studying divergence.

To accomplish the first objective, nine cantilevered wing models were tested in the Langley Transonic Dynamics Tunnel (TDT). Seven of these models were flat-plate wings tested to determine the effects of aspect ratio and leading-edge wing sweep on divergence speeds in the subsonic region. Two additional models were constructed with different airfoil shapes to determine the effort of airfoil section on the divergence boundary in the transonic region. In this paper, the models are described, test results are presented, and calculated results are presented for comparison with experimental results.

The second objective was accomplished by developing and evaluating subcritical response techniques for predicting the divergence condition (dynamic pressure) using response measurements made below divergence. In this paper, six different methods are described, and an application of each is presented. Two of these methods were recently developed by Wilmer H. Reed III, and their derivations are presented in appendix B. In addition, two divergence "stopper" devices were developed to prevent model damage if divergence occurs during wind-tunnel tests. These two devices, a "flow-diverter" and a "model-constrainer," are also described.

Use of trade names or names of manufacturers in this report does not constitute an official endorsement of such products or manufacturers, either expressed or implied, by the National Aeronautics and Space Administration.

SYMBOLS

A	peak dynamic amplitude, V
AR	aspect ratio, $2(s/c)$
C	strain-gage proportionality factor, V/deg
c	chord length, m
$c_{l,o}$	lift coefficient at $\alpha = 0$
c_{l_α}	lift-curve slope
$c_{m,ac}$	moment coefficient about aerodynamic center
e	distance between elastic axis and aerodynamic center, m
f	frequency, Hz

k	torsional spring constant, N-m/deg
l	lift per unit span, N/m
M	Mach number
m_{ac}	moment about aerodynamic center, N-m
m_e	moment about elastic axis, N-m
P	compression load, N
P_{cr}	critical buckling load, N
q	dynamic pressure, kPa
q_D	divergence dynamic pressure, kPa
s	semispan length, m
α_e	angle of attack due to aerodynamic loads, deg
α_R	root angle of attack, deg
α_o	angle of attack when $m_e = 0$ ($\varepsilon = 0$), deg
$\bar{\alpha}$	$= \alpha_R - \alpha_o$, deg
δ	deflection, mm
δ_o	initial deflection, mm
Δ	divergence index parameter
ε	mean strain-gage output, V
λ	slope of ε-versus-α_R curve, V/deg
Λ	leading-edge sweep angle, deg (forward sweep is negative)
ρ	air density, kg/m^3

Subscripts:

exp	experimental
n	nth value
r	rth value

TEST APPARATUS AND PROCEDURES

Models

Geometry.- Seven semispan flat-plate wing models were tested during the static divergence investigation. All the wings were untapered and had a semispan length of 0.508 m. In planform, the models differed only in aspect ratio and leading-edge wing sweep. The models had full-span aspect ratios of 4.0 and 8.0 and wing sweep angles of 0°, -7.5° (only $\mathcal{R} = 8.0$), -15°, and -30°. The planform geometries for these models are shown in figure 1.

Two additional models with 10-percent-thick airfoil sections were tested. These models had a planform identical to the flat-plate models with aspect ratios of 4.0 and wing sweep angles of -15°. One had a conventional airfoil (NACA 64A010); the other had an uncambered (symmetric) supercritical airfoil section.[2] These two models, in conjunction with a flat-plate model with similar planform, were used to determine effects of airfoil section on the divergence boundary in the transonic region.

Construction.- All the models were constructed of 2.29-mm-thick aluminum alloy plate. For the flat-plate models, the leading and trailing edges were rounded to a semicircular shape. For the models with airfoil sections, a lightweight plastic foam was attached to the aluminum plate and then shaped to give the desired airfoil section. Transition strips (No. 46 carborundum grit) with a width of 0.025 chord were added along the 5-percent chord line on both the upper and lower surfaces of all the models to assure that the boundary layer was turbulent.

Instrumentation.- Each model was instrumented with resistance-wire strain-gage bridges located near the wing root. The bridges were oriented to be sensitive to either bending or torsional strains.

Vibration characteristics.- The first three natural frequencies - first bending, second bending, and torsion - were measured for each wing model. For comparison, mode shapes and frequencies were calculated for the flat-plate models using the SPAR finite element structural analysis computer program (ref. 6). Both measured and calculated frequencies for the flat-plate models are presented in table I. The associated calculated node lines are shown in figure 2 and were substantiated by abbreviated measurements. In figure 2, the torsion mode is the second mode for aspect-ratio-4.0 models, and the second bending mode is the third mode. This order is reversed for the aspect-ratio-8.0 models.

Model Mount and Divergence Stoppers

The model wings were cantilever mounted outside the tunnel-wall boundary layer on an I-beam support fixture attached to a remotely controlled turntable.

---

[2]This section was an early supercritical airfoil (designated NASA SC(2)-0010) derived from the family of cambered airfoils presented in reference 5.

A splitter plate was mounted to the support fixture to provide a reflection plane for the model. The turntable provided the capability of changing the wing angle of attack during the test. A photograph showing the model mounting arrangement is presented in figure 3.

Because of the potentially destructive nature of aeroelastic instabilities, precautions are commonly taken to minimize the risk of model damage during wind-tunnel tests. In the present study, two devices (each attached to the support fixture) were developed for preventing excessive model deformations during divergence. These devices are described in detail in appendix A. One device, called a "flow-diverter" (shown in fig. 4), is simply a hinged plate that deflects the airstream when it is deployed. Deflecting the airflow changes the relative angle between the flow and the wing leading edge and in effect reduces the forward sweep. It is shown later that this situation yields a higher divergence dynamic pressure. In addition, the dynamic pressure is decreased by the shielding effect that the flow-diverter offers; that is, the wing is exposed to lower velocities in the wake of the device. The other device, called a "model-constrainer" (shown in fig. 5), consists of a pair of arms that are hinged to the support fixture at one end and have wheels or rollers at the other end. When this device is deployed, the arm swings out the span of the model, and the wheels bear on the wing upper and lower surfaces to stiffen the model and return it to its undeformed shape. Both devices were demonstrated to prevent divergence from occurring at dynamic pressures at least 33 percent greater than the wing-alone divergence dynamic pressure.

Wind Tunnel

The present investigation was conducted in the Langley Transonic Dynamics Tunnel (TDT). The TDT is a continuous-flow, single-return tunnel with a 4.88-m square test section (with cropped corners) having slots in all four walls (ref. 7). The flow is generated by a motor-driven fan. The tunnel is equipped to use either air or Freon 12 as the test medium at pressures which vary from near vacuum to slightly above atmospheric. The range of Mach numbers is from near zero to 1.2. Both the density and the test-section Mach number are continuously controllable. The tunnel is equipped with four hydraulically activated, quick-opening bypass valves. When model instability is encountered, these valves are actuated to rapidly reduce the dynamic pressure and Mach number in the test section.

Test Procedures

Low-speed tests.- Divergence tests of the flat-plate wings, evaluation of the subcritical response divergence prediction techniques, and evaluation of the divergence stoppers were conducted simultaneously in air at atmospheric pressure. For these low speed tests, the determination of a typical divergence point proceeded in the following manner. With the angle of attack set at some low positive value to keep the model lightly loaded in a single direction, the fan speed was increased to the desired test-section dynamic pressure. This initial dynamic pressure was chosen to be relatively far below the divergence condition. At this dynamic pressure, data were collected to evaluate the sub-

critical response methods. This process involved stepping the model through a range of angles of attack and acquiring data at each angle. The model was then returned to its original position, tunnel speed was increased to a slightly higher dynamic pressure, and model response measurements were repeated. This stepwise increase in dynamic pressure was continued until divergence was reached. When divergence occurred, damage to the model was prevented either by deploying a divergence stopper (if one had been installed), or by actuating the four bypass valves in the tunnel.

Transonic tests.- Tests conducted in the transonic regime used Freon 12 as the test medium. The following procedure was used to vary Mach number and dynamic pressure (shown in fig. 6). With the tunnel evacuated to a low stagnation pressure, the fan speed was increased until the desired maximum test Mach number was reached. The dynamic pressure at this tunnel condition was relatively far below the divergence dynamic pressure. Subcritical response data were collected at this tunnel condition in the same manner as described for the low-speed tests. Next, while the Mach number was held constant, the test-section dynamic pressure was increased by bleeding additional Freon 12 into the tunnel through an expansion valve. When the desired dynamic pressure was obtained, tunnel-flow conditions were held constant, and subcritical response data were again acquired. This process was repeated until either divergence was reached or sufficient subcritical data were obtained to predict the divergence condition at this Mach number. During this process, the flow-diverter divergence stopper was used to protect the model from damage.

To define the divergence condition at another Mach number, the fan speed was decreased until the desired Mach number was obtained. With the Mach number again held constant, the procedure of acquiring data and stepping the dynamic pressure was repeated in the manner just described. In this way, the divergence boundary was defined throughout the region of interest.

Data acquisition.- During the tests, the output signals from the model strain-gage bridges were recorded on oscillograph strip recorders. The Spectral Dynamics Corporation 330A Spectrascope (spectrum analyzer) was used to determine frequencies and peak amplitudes. The tunnel data acquisition system was used to calculate and display the parameters needed for the subcritical response prediction techniques.

TEST RESULTS AND DISCUSSION

Experimental results acquired during the testing of models can be divided into two categories: (1) data from model tests at low speeds in air, and (2) data from model tests at transonic speeds in Freon 12.

Low-Speed Results

All flat-plate models were tested at low speeds in air at standard atmospheric pressure. Results of these tests are presented in figures 7 and 8 for the aspect-ratio-4.0 and aspect-ratio-8.0 wings, respectively, as plots of dynamic pressure versus wing sweep. Calculated flutter and divergence bound-

aries are shown with each set of data. In the calculations, linear unsteady aerodynamics (ref. 8) at a Mach number of 0.3 were used in a traditional flutter analysis (ref. 9).

Aspect-ratio-4.0 wings.- The calculated results presented in figure 7 for the aspect-ratio-4.0 models are similar to the results presented by Diederich and Budiansky (ref. 10) and show that two distinct instabilities, divergence and flutter, exist with varying wing sweep. As shown in the figure, the calculated divergence dynamic pressure increases as the wing sweep changes from -30° to 0°. Conversely, the calculated flutter dynamic pressure decreases as the wing sweep changes from -30° to 0°. The flutter mode is primarily wing first bending but contains a small amount of coupling with torsion and second bending. The calculated flutter frequency for the unswept ($\Lambda = 0^{\circ}$) model is 18.5 Hz.

The measured divergence and flutter points shown in figure 7 are in good agreement with the calculations. The 15° and 30° forward-swept models experienced divergence instabilities. The unswept model experienced a flutter instability and had a measured flutter frequency of 21.0 Hz.

Aspect-ratio-8.0 wings.- Calculated results presented in figure 8 for the aspect-ratio-8.0 models appear more complex than results for the aspect-ratio-4.0 models. Three separate calculated instability boundaries are shown for these wings: a divergence boundary and two flutter boundaries. Two of the instability boundaries are similar to those described for the aspect-ratio-4.0 wings. One is a divergence boundary in which calculated divergence-dynamic pressure increases as the wing sweep changes from -30° to 0°. The other is the upper calculated flutter boundary in which the flutter dynamic pressure decreases as the wing sweep changes from -30° to 0°. This flutter mode is primarily wing first bending but contains a small amount of coupling with second bending and torsion. The calculated flutter frequency for the unswept model is 28.9 Hz.

The other calculated flutter boundary shows up as a "hump mode" in the analysis. Traditionally, the hump mode is characterized by the damping-versus-velocity curve shown in sketch (a). This curve moves up or down with variations in air density ρ. (At some densities, for example, ρ_1, the hump mode lies

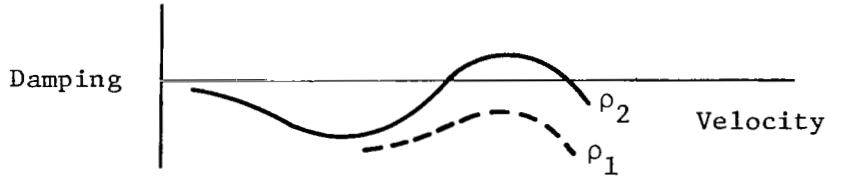

Sketch (a)

totally below the zero-damping line and therefore is not unstable.) In figure 8, however, the hump mode seems to be a function of wing sweep and disappears for sweep angles greater than 0°. The flutter mode is primarily wing second bending but has a small amount of coupling with torsion and first bending. Calculated flutter frequencies for the 7.5° forward-swept and the unswept models are 48.1 and 47.9 Hz, respectively.

Measured divergence and flutter points shown in figure 8 are in good agreement with calculated results. The 15° and 30° forward-swept models experienced divergence instabilities. The 7.5° forward-swept model experienced a flutter instability at 46.4 Hz that had the appearance of a second wing bending mode. (A node line existed near the wing tip.) This instability agrees with the calculated hump mode. The unswept model experienced a flutter instability with a flutter frequency of 30.0 Hz. A region of significant response was observed, however, from $q = 4.1$ to 6.2 kPa in which the primary model response frequency was about 45.0 Hz. This is probably a region of low damping for the hump mode.

Transonic-Speed Results

Three models were tested in the transonic-speed range in Freon 12 up to $M = 0.9$. The purposes of these tests were (1) to acquire transonic data and (2) to determine the effect of airfoil shape on divergence. All these models had an aspect ratio of 4.0 and a wing sweep of -15°. The models had three different airfoil shapes - flat plate, conventional, and supercritical. In figure 9, the measured divergence dynamic pressure for each model is presented as a ratio to the dynamic pressure at $M = 0.6$ for different values of Mach number. As shown in the figure, the region of minimum divergence dynamic pressure, or the so-called "transonic dip," occurs at an appreciably lower Mach number for the conventional airfoil than for the supercritical airfoil. Also, the width of transonic dip appears to be narrower for the conventional airfoil than for the supercritical airfoil. The flat-plate results show a decrease in dynamic pressure in the transonic range, but a minimum was not observed. Analysis using linear aerodynamic theory shows a transonic boundary in good agreement with measured flat-plate results. Linear theory is therefore useful for the analysis of thin wings. For accurate analysis of thick wings in the transonic region, however, a more sophisticated theory is needed.

SUBCRITICAL RESPONSE TECHNIQUES - DESCRIPTION AND EVALUATION

Subcritical response testing techniques are frequently used in flutter testing to predict a flutter instability before it occurs (ref. 11). Because flutter is often a destructive phenomenon, such predictive methods allow an approach to the instability with a minimum risk of damaging the model. In many cases, confidence in these methods is high enough to define a flutter instability boundary without actually experiencing flutter.

A similar procedure was desired for use in divergence testing. Therefore, several methods were investigated to predict static divergence based on the response of the model at dynamic pressures below the stability boundary. These methods can be classified as either static or dynamic in nature. The static methods include inverse mean strain, Southwell, divergence index, and constant load. The dynamic methods include inverse peak amplitude and frequency. For all these methods, data were acquired and analyzed in the transonic region at a constant Mach number with varying dynamic pressure. In this manner, shifts in center of pressure due to Mach number changes were eliminated from the data.

The six methods were evaluated on several models at various Mach numbers with similar results. For illustrative purposes, however, only the Mach 0.8 results for the aspect-ratio-4.0 flat-plate model with a wing sweep of -15° are presented. At this Mach number, the model experimentally diverged at a dynamic pressure of 2.52 kPa. Discussion and evaluation of each subcritical method follows. Two new methods, divergence index and constant load, are derived in appendix B.

Static Methods

The basic data that were used in the static prediction methods are presented in figure 10. Data for a range of model angles of attack were acquired in the manner previously described in the section "Test Procedures." A first-order least-squares fit was used to calculate the slope λ and the angle α_o of the equation $\varepsilon = \lambda(\alpha_R - \alpha_o)$ for the data at each dynamic pressure.

Inverse mean strain method.- One of the simplest prediction methods is the inverse mean strain technique, which evaluates the change in the reciprocal of the mean strain with the change in dynamic pressure. This method takes advantage of the fact that the wing tip deflection, thus, the root bending moment and strain, tend toward infinity as the divergence condition is approached. Conversely, the inverses of the parameters tend toward zero at divergence. Therefore, the divergence dynamic pressure is the point at which the inverse mean strain is zero and is predicted by extrapolating a second-order least-squares fit of the subcritical data. Because the data most often displayed a "concave up" shape (positive second derivative), the fit was required to be "concave up" or linear in the limiting case.

In figure 11, the results of applying this method at model angles of attack of 0.09° and 0.17° are presented. For these cases, the predicted dynamic pressure is within 4 percent of the measured value.

Southwell method.- This method was developed by R. V. Southwell in 1932 to predict the critical buckling load of a column loaded axially in compression (ref. 12). In 1945, it was suggested by Alexander Flax (ref. 13) that this method could be used in studying aeroelastic problems like divergence. The Southwell equation is

$$\delta = \frac{P\delta_o}{P_{cr} - P} \tag{1}$$

where δ_o is the initial deflection measured laterally at the middle of the column, δ is the deflection measured from δ_o for each axial load P, and P_{cr} is the critical buckling load.

Equation (1) is similar in form to the equation that characterizes the elastic deflection of an aeroelastic system as divergence is approached. (See,

for example, eq. (B10a) in appendix B.) For the aeroelastic system the corresponding equation becomes

$$\alpha_e = \frac{q\bar{\alpha}}{q_D - q} \tag{2}$$

where $\bar{\alpha}$ is the initial wing root angle of attack, α_e is the angle of attack due to aerodynamic load, q is the dynamic pressure, and q_D is the divergence dynamic pressure. When α_e is proportional to the model strain measurement ε through the equation $\alpha_e = C\varepsilon$, where C is the proportionality factor, equation (2) can be put in the form

$$\varepsilon = q_D\left(\frac{\varepsilon}{q}\right) - \frac{\bar{\alpha}}{C} \tag{3}$$

which is linear in ε and ε/q with slope q_D. In figure 12, data are presented in this form for two angles of attack. A first-order least-squares fit of the data was used to predict the divergence dynamic pressure (slope of the line) in these cases. The predicted values are within 4 percent of the measured divergence dynamic pressure.

An advantage in using this method is that the basic data (fig. 10) only need to be acquired at a single angle of attack. However, care must be taken in choosing this angle so that the allowable strength loads of the model are not exceeded before the divergence condition is identified.

The prediction method can be improved if all the basic data (fig. 10) are used in the method. In this case, the method is modified so that the slope λ (where $\lambda = \varepsilon/\bar{\alpha}$) of the basic data is used instead of a value of strain at a single angle of attack. Equation (3) then becomes

$$\lambda = q_D\left(\frac{\lambda}{q}\right) - \frac{1}{C} \tag{4}$$

In figure 13, a result of applying this method is presented as a plot of λ versus λ/q. Again, a linear least-squares fit was used to predict the divergence dynamic pressure (slope), which is less than 2 percent lower than the measured value.

Divergence index method.- The divergence index method is derived in appendix B. This method is based on the same equation as the Southwell method; however, the testing procedure and graphical presentation of the test data are different. The test procedure consists of measuring model strain as the angle

of attack is varied for a series of constant dynamic pressures (shown in fig. 10). At each dynamic pressure q_n, the slope λ_n is measured and the divergence index parameter Δ_n is computed from the equation

$$\Delta_n = \frac{1 - \left(q_n/q_r \right)}{1 - \left(\lambda_n/\lambda_r \right)} \tag{5}$$

where the subscript r denotes a reference condition, which is usually associated with the lowest value of dynamic pressure. The number of Δ_n values that can be calculated is 1 less than the total number of different dynamic pressures for any given reference condition.

As shown in appendix B, Δ is related to q by the following equation:

$$\Delta = 1 - \left(\frac{1}{q_D} \right) q \tag{6}$$

This is a straight line which passes through unity at $q = 0$ and intersects the q-axis at the predicted divergence dynamic pressure q_D.

Results of applying this method are presented in figure 14. From the basic data (fig. 10), four values of Δ were calculated using five values of dynamic pressure. The divergence dynamic pressure was determined from equation (6) by applying a first-order least-squares fit to the Δ versus q data and calculating the q-intercept. The least-squares fit was forced through unity along the Δ-axis. The predicted divergence dynamic pressure is within 1 percent of the measured value.

This method appears to give accurate results even for values of dynamic pressure far removed from the divergence condition. This is attributed to the inclusion of the Δ-intercept in the data. Much accuracy is gained in the least-squares fit by having this unity point so far removed from the rest of the data.

Constant-load method.- The final static method to be described is the constant-load method, also derived in appendix B. In this method, the aerodynamic load measured by the strain gages on the model is held constant as the dynamic pressure is increased toward a divergence condition. To maintain this constant load, the angle of attack is varied.

This method is based on the same equation as that used in the derivation of the divergence index method. The equation for this method is obtained by rearranging equation (3):

$$q\bar{\alpha} = (-C\varepsilon)q + C\varepsilon q_D = C\varepsilon(q_D - q) \tag{7}$$

By defining ε to be constant, the equation is linear in $q\bar{\alpha}$ and q. The divergence dynamic pressure q_D occurs when $q\bar{\alpha}$ is equal to zero or, in other words, when $q\bar{\alpha}$ crosses the q-axis.

In applying the constant-load method to the basic data in figure 10, the values of $\bar{\alpha}$ are determined by first extrapolating the data at each dynamic pressure to the no-load ($\varepsilon = 0$) condition and then using the relationship $\bar{\alpha} = \alpha_R - \alpha_O$. The results of applying the method are presented in figure 15. A linear least-squares fit was used to extrapolate to $q\bar{\alpha} = 0$ to predict the divergence dynamic pressure. The predicted divergence dynamic pressure is within 1 percent of the measured value.

Dynamic Methods

In addition to the static methods previously explained, two methods of analyzing the dynamic signal from the strain-gage measurements were investigated to determine their accuracy in predicting divergence. Both methods utilized the spectrum analyzer to obtain the data. The model was tested at a no-load condition and was randomly excited by the airstream.

Inverse peak amplitude method.- This method is based on the assumption that the dynamic amplitude of the divergence model tends toward infinity as the divergence condition is approached. The inverse of the amplitude, therefore, will approach zero. A similar approach was first used by Sandford et al. (ref. 14) to predict the flutter instabilities of an aeroelastic model.

This method of divergence prediction was applied in the following manner. The data for the dynamic methods were obtained at the same time as those for the static method. At each dynamic pressure, a spectrum of the dynamic response of the model in a no-load condition was recorded. The wing first bending mode was identified from the spectrum, and its peak response was measured. In figure 16, results of applying this method are presented. The inverses of the peak measurements are plotted against dynamic pressure. The data were extrapolated using a second-order least-squares fit to predict the divergence dynamic pressure, which is the value of the point where the inverse equals zero. The predicted divergence pressure is within 2 percent of the measured value.

Frequency method.- Another method which uses the spectrum of the dynamic response is based on the fact that the frequency of the divergence mode is zero at divergence. (For this reason, the instability is called static divergence.) Frequencies from spectrum data are used to "track" the wing first-bending mode frequency from the no-wind value to zero.

In figure 17, the result of applying this method is presented. A second-order least-squares fit was used to predict the divergence dynamic pressure which occurs when the frequency equals zero. The predicted divergence dynamic pressure is within 1 percent of the measured value.

Remarks on Prediction Methods

In general, the static methods seemed to consistently give better quality data than the dynamic methods. The subcritical data from static methods were more repeatable and showed less scatter throughout the dynamic pressure range. It was particularly difficult to acquire good quality frequencies and dynamic amplitudes for data below 1.0 Hz. The methods which use a linear fit of the subcritical data for predictions were more accurate than those which use a second-order fit. The linear fit methods converged to accurate predictions more rapidly (farther from q_D) than did the nonlinear methods. The Southwell, divergence index, and constant-load methods consistently yielded similar predictions. This situation appears to be true because the three methods were derived from the same basic equation (eq. (2)). Of these three static methods, the Southwell data contained the least amount of scatter. Although the example given previously in the paper shows that the inverse mean strain method is accurate, other examples showed it to be conservative by underpredicting the divergence dynamic pressure. This result may be due to the choice of the second-order curve fit for extrapolation. A hyperbolic curve fit, for example, might be more appropriate.

CONCLUSIONS

An experimental study of the static aeroelastic divergence of forward-swept wings has been described. Nine plate models, two of which had airfoil sections attached, were used in the study. The models were wind-tunnel tested at low speeds in air, and at transonic speeds in Freon 12 to determine divergence characteristics. Subcritical response testing techniques for predicting divergence were formulated and evaluated. Two divergence stoppers were developed and tested to determine their effectiveness in protecting a model at divergence.

The important results follow:

1. A divergence-stopper device, such as the flow-diverter or the model-constrainer, can be effectively used during divergence testing to help protect the model from destruction.

2. Linear theory accurately predicts the aeroelastic behavior, including divergence and flutter, of thin forward-swept wings. For accurate predictions of divergence characteristics of thick wings in the transonic region, a more sophisticated theory is needed.

3. The aeroelastic divergence boundary can be accurately defined using subcritical response testing techniques.

Langley Research Center
National Aeronautics and Space Administration
Hampton, VA 23665
June 16, 1980

APPENDIX A

DIVERGENCE STOPPERS

Wind-tunnel testing of aeroelastic models often jeopardizes the model because instabilities such as flutter and divergence produce large, rapidly increasing model deformations that can lead to structural failure. It is common practice, therefore, to take precautions during testing to minimize the risk of model damage when an aeroelastic instability is encountered. As mentioned in the body of the paper, the application of subcritical response test techniques is one way to minimize risks. However, even in applying subcritical methods, it is usually necessary to determine at least one instability point to validate the method.

Another means of reducing the risk of model damage is to conduct aeroelastic model studies in wind tunnels that have a means of rapidly reducing flow dynamic pressure. These methods include spoilers that are deployed in the tunnel diffuser to provide a choking effect and valve-piping arrangements that are used to short circuit the flow between the low-speed leg of the tunnel and the test-section plenum chamber. The spoiler is usually very effective, but because large loads can develop on the device when it is deployed, the spoiler is usually used only in small tunnels. The valve-piping system is more applicable to large tunnels (i.e., the Langley Transonic Dynamics Tunnel) and does not have as much effect as the spoiler. However, in both cases, the wind tunnel must be equipped with the device before it can be used. Both require extensive modifications to the tunnel.

Other methods of minimizing the risk of model damage include physically restraining the model with cables which are normally slack but become taut when the model deflection reaches a preset value. Although such restraint methods are usually effective in minimizing model damage, the presence of cables distorts the flow over the model and may change its aeroelastic characteristics.

In the present study two devices, or instability stoppers, that can be used to prevent damage to aeroelastic wind-tunnel models during testing were developed and demonstrated successfully. Both devices are mechanically simple, capable of rapid actuation at any test condition, adaptable for use in any wind tunnel, noninterfering with the flow field around the model, and noninterfering with the dynamic characteristics of the model. For purposes of discussion, one device is referred to as the flow-diverter, and the other is referred to as the model-constrainer. The purpose of this appendix is to describe each of these devices.

Flow-Diverter Device

The flow-diverter is illustrated schematically in figures 18 and 19. This device was developed for use in divergence studies of forward-swept wings. The simplest form of this device is a hinged plate that is mounted upstream of the

model. In the stored position (fig. 18), the plate is recessed in the wind-tunnel wall, or splitter plate, so that there is no aerodynamic interference produced by the plate. For thin plates, a flush mounting with the wind-tunnel wall is satisfactory. When the device is actuated (fig. 19), the plate is deployed into the airstream by a quick acting, remotely controlled, pneumatic or hydraulic actuator. When the plate is deployed, the flow is diverted over the outboard portion of the model, which has the effect of reducing the sweep angle of the model. This reduction in sweep angle increases the divergence speed. Furthermore, the dynamic pressure is decreased by the shielding effect that the flow-diverter offers; the wing is exposed to lower velocities in the wake of the device.

For applications in which the model is mounted off the wind-tunnel wall on a splitter plate, two plates may be used (shown in fig. 20). The inner plate diverts the flow behind the splitter plate so that the air is channeled over the inboard portion of the model through a hole in the splitter plate. The purpose of this inner plate is to relieve the suction pressure behind the outer plate, which functions as the previously described single-plate device, and to allow it to be more effective in turning the flow. If a more gradual turning of the flow is required, a multisegment outer plate can be used. A two-segment device is shown in figure 21.

Both the single-plate (fig. 18) and the two-plate (fig. 20) flow diverters were used in the present study. Both applications proved effective in rapidly returning the model to an undiverged condition. Although the static deformation was reduced, the models did experience some random dynamic response that was apparently produced by turbulent flow off the edges of the outboard plate. The random response was less for the two-plate case, and was not considered to be excessive in either case.

Model-Constrainer Device

The model-constrainer, which is shown schematically in figure 22, is applicable to both flutter and divergence testing. As illustrated in the figure, the device consists of an arm that is hinged at one end to the splitter plate (or tunnel wall). A pair of soft wheels, or rollers, is attached to the other end of the arm. When the device is actuated, the arm rotates away from the wall, and the wheels roll along the upper and lower surfaces of the model, thus returning the model to its undeformed shape and preventing either static or dynamic model deflection. The device is operated by a remotely controlled pneumatic, or hydraulic, actuator. To minimize aerodynamic interference, the device can be recessed in the wind-tunnel wall, splitter plate, or fuselage half-body, depending on the application. Although the illustrations are for application to a forward-swept wing, the device is equally applicable to aft-swept wings for use as a flutter stopper. For aft-swept wings, the device would be mounted downstream of the model.

The model-constrainer was shown to be very effective in restraining the model when divergence occurred. An advantage of this device over the flow-diverter was that the models did not experience random excitation.

APPENDIX B

DERIVATION OF TWO METHODS FOR PREDICTING STATIC DIVERGENCE OF WINGS FROM SUBCRITICAL TEST DATA

Wilmer H. Reed III
Langley Research Center

Idealized Aeroelastic System

In this appendix, a derivation is given for the testing techniques referred to in the body of the paper as the "divergence index" method and the "constant-load" method. These methods are developed on the basis of a simplified aeroelastic system which is assumed to represent a "typical section" of a flexible wing. As shown in figure 23, the typical section consists of a rigid airfoil mounted on a torsional spring located at the effective elastic axis of the system. The base of the spring can be inclined at an angle α_R relative to the flow direction as a means of lift control. The angle α_e represents the twist of the spring due to aerodynamic loads on the airfoil. Thus, the aerodynamic angle of attack of the airfoil is the rigid-body angle plus an increment due to aeroelastic deformation

$$\alpha = \alpha_R + \alpha_e \tag{B1}$$

The lift force per unit span l acting at the airfoil center of pressure and the moment about the aerodynamic center m_{ac} are, respectively,

$$l = qc\left(c_{l,o} + c_{l_\alpha}\alpha\right) \tag{B2}$$

$$m_{ac} = qc^2 c_{m,ac} \tag{B3}$$

where $c_{m,ac}$, by definition, is independent of angle of attack.

Thus, the aerodynamic moment about the elastic axis is

$$m_e = el + m_{ac} \tag{B4}$$

where e is the distance between the aerodynamic center and the elastic axis (e is positive when the aerodynamic center is forward of the elastic axis).

For a flat-plate airfoil in two-dimensional, incompressible flow, $c_{l,o}$ and $c_{m,ac}$ are zero, and equation (B4) becomes simply

$$m_e = ecqc_{l_\alpha}\left(\alpha_R + \alpha_e\right) \tag{B5}$$

To retain the simplicity of this form of the moment equation for the more general case in which $c_{l,o}$ and $c_{m,ac}$ are nonzero, it is convenient to introduce an angle $\bar{\alpha}$ shown in figure 23 and defined as

$$\bar{\alpha} = \alpha_R - \alpha_o \tag{B6}$$

where α_o is the rigid-body angle of attack for which the aerodynamic moment about the elastic axis is zero. The value of α_o required to satisfy the condition $m_e = 0$ is, from equations (B2), (B3), and (B4), found to be

$$\alpha_o = -\frac{(e/c)c_{l,o} + c_{m,ac}}{(e/c)c_{l_\alpha}} \tag{B7}$$

The general form of equation (B5) now becomes

$$m_e = ecqc_{l_\alpha}\left(\bar{\alpha} + \alpha_e\right) \tag{B8}$$

This is the aerodynamic moment about the elastic axis which is balanced by the torsion spring so that

$$k\alpha_e = m_e \tag{B9}$$

Substituting equation (B8) into equation (B9) and solving for α_e gives

$$\alpha_e = \frac{q\bar{\alpha}}{q_D - q} \tag{B10a}$$

where

$$q_D = \frac{k}{ecc_{l_\alpha}} \tag{B10b}$$

Because the denominator of equation (B10a) vanishes as $q \to q_D$, causing the twist of the spring to become infinitely large, q_D is the dynamic pressure at divergence. Furthermore, because dynamic pressure is always a positive real

quantity, equation (B10b) indicates that divergence can occur only when $e > 0$, i.e., when the elastic axis is behind the aerodynamic center.

From equation (B10a) the divergence dynamic pressure may be expressed in terms of the experimentally determined quantities q, $\bar{\alpha}$, and α_e.

$$q_D = q\left(1 + \frac{\bar{\alpha}}{\alpha_e}\right) \tag{B11}$$

To relate divergence predictions for an actual wing structure to those derived for the idealized two-dimensional section treated here, the quantity α_e in equation (B11) is assumed to be proportional to the output of a strain gage on the wing structure which senses elastic deformation of the wing due to load as in the equation

$$\alpha_e = C\varepsilon \tag{B12}$$

A typical set of data taken during the test of a wing structure is illustrated in sketch (b). The data are linear and have a slope λ such that

$$\lambda = \frac{d\varepsilon}{d\alpha_R} = \frac{\varepsilon}{\alpha_R - \alpha_o} = \frac{\alpha_e/C}{\bar{\alpha}} \tag{B13}$$

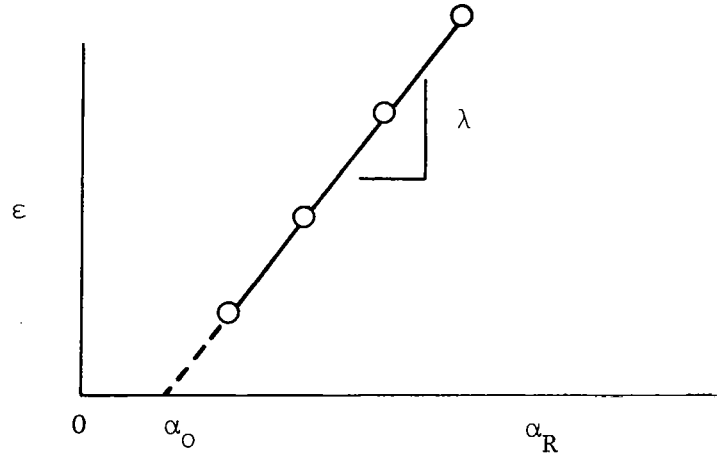

Sketch (b)

Divergence Index Method

The test procedure for the divergence index method consists of measuring a strain-gage output as the angle of attack is varied at constant dynamic pres-

sure. A series of such measurements are taken at successively higher dynamic pressures, $q_1, q_2, \ldots, q_n$, holding Mach number constant if compressibility effects are significant. Letting λ_n be the slope measured at q_n and using equations (B12) and (B13), it is easily shown that

$$\lambda_n = \frac{q_n}{C(q_D - q_n)} \tag{B14}$$

Letting λ_r and q_r be values for a reference condition that is well below the expected divergence condition, the ratio λ_n/λ_r is formed to eliminate C such that

$$\frac{\lambda_n}{\lambda_r} = \frac{q_n}{q_r}\frac{q_D - q_r}{q_D - q_n} \tag{B15}$$

where $q_r < q_n < q_D$. Solving equation (B14) for q_D yields

$$q_D = q_n \frac{(\lambda_n/\lambda_r) - 1}{(\lambda_n/\lambda_r) - (q_n/q_r)} \tag{B16}$$

Thus, for each set of ε-versus-α_R measurements taken at different values of q, a new prediction of q_D is obtained from equation (B16).

To provide a convenient graphical display which further aids in the estimation of the divergence dynamic pressure from subcritical data, a so-called "divergence index" parameter is defined as follows:

$$\Delta = 1 - \frac{q}{q_D} \tag{B17}$$

Values of Δ are computed from the following equation:

$$\Delta_n = \frac{1 - (q_n/q_r)}{1 - (\lambda_n/\lambda_r)} \tag{B18}$$

An application of the equations to a set of subcritical data is illustrated in sketch (c). When plotted against q, the parameter Δ decreases linearly with negative slope $(-q_D^{-1})$ and crosses the q-axis at divergence.

APPENDIX B

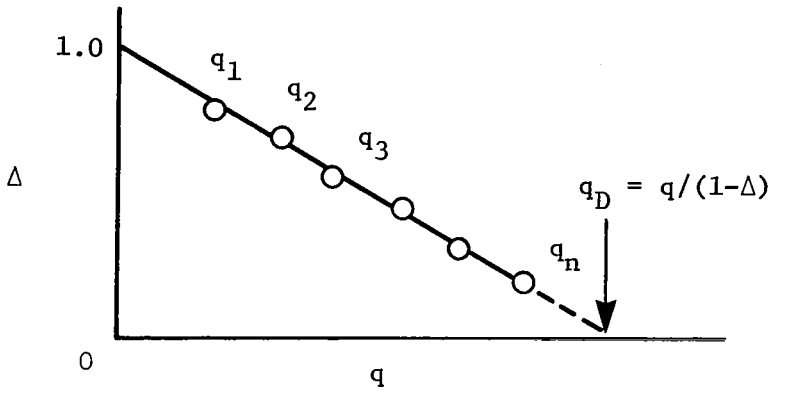

Sketch (c)

When the measured data contain scatter, the accuracy of divergence prediction may be enhanced by applying the method of least squares. In this case, the unknown q_D would be determined from a set of n equations $(n > 2)$ which relate $q_1, q_2, \ldots, q_n$ to the observed slopes $\lambda_1, \lambda_2, \ldots, \lambda_n$.

Constant-Load Method

This method involves varying the dynamic pressure while controlling the rigid-body angle $\bar{\alpha}$ so as to maintain constant strain measurement ε. A practical advantage of this method over some others is that it minimizes the risk of overloading the model as the divergence condition is approached during tests. Because the aerodynamic load is held constant (α_e = Constant), from equation (B10) the derivative of $q\bar{\alpha}$ with respect to q, becomes

$$\frac{dq\bar{\alpha}}{dq} = -\alpha_e \tag{B19}$$

An illustration of this method is shown in sketch (d), which illustrates that $q\bar{\alpha}$ versus q plots as a straight line with a negative slope of $-\alpha_e$. Divergence is indicated when $q\bar{\alpha} = 0$, that is, when $\bar{\alpha} = 0$ or, in other words, when the load is developed entirely by the angle of attack associated with the aeroelastic deformation α_e.

APPENDIX B

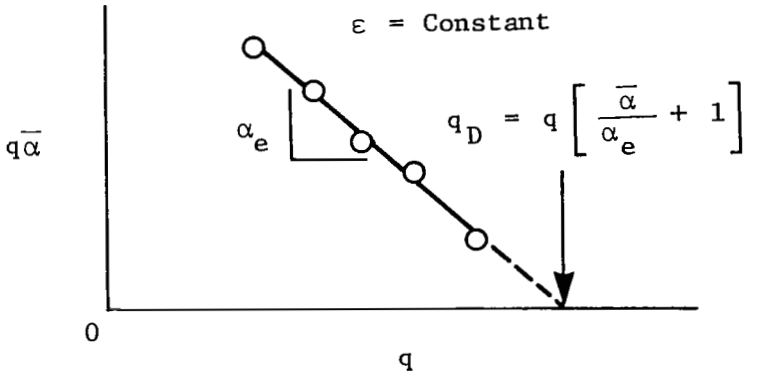

Sketch (d)

REFERENCES

1. Forward-Swept Wing Potential Studied. Aviat. Week & Space Technol., vol. 110, no. 5, Jan. 29, 1979, pp. 126-127.

2. Holzbaur, Siegfried: Swept-Forward Wings. Interavia, vol. V, no. 7, 1950, pp. 380-382.

3. Taylor, John W. R., ed.: Jane's All the World's Aircraft, 1970-71. McGraw-Hill Book Co., c.1970.

4. Krone, Norris J., Jr.: Divergence Elimination With Advanced Composites. AIAA Paper No. 75-1009, Aug. 1975.

5. Whitcomb, Richard T.: Review of NASA Supercritical Airfoils. ICAS Paper No. 74-10, Aug. 1974.

6. Whetstone, W. D.: SPAR Structural Analysis System Reference Manual - System Level 11. Volume 1: Program Execution. NASA CR-145098-1, 1977.

7. Yates, E. Carson, Jr.; Land, Norman S.; and Foughner, Jerome T.: Measured and Calculated Subsonic and Transonic Flutter Characteristics of a 45° Sweptback Wing Planform in Air and in Freon-12 in the Langley Transonic Dynamics Tunnel. NASA TN D-1616, 1963.

8. Watkins, Charles E.; Woolston, Donald S.; and Cunningham, Herbert J.: A Systematic Kernel Function Procedure for Determining Aerodynamic Forces on Oscillating or Steady Finite Wings at Subsonic Speeds. NASA TR R-48, 1959.

9. Desmarais, Robert N.; and Bennett, Robert M.: User's Guide for a Modular Flutter Analysis Software System (FAST Version 1.0). NASA TM-78720, 1978.

10. Diederich, Franklin W.; and Budiansky, Bernard: Divergence of Swept Wings. NACA TN 1680, 1948.

11. Flutter Testing Techniques. NASA SP-415, 1976.

12. Southwell, R. V.: On the Analysis of Experimental Observations in Problems of Elastic Stability. Proc. Roy. Soc. (London), ser. A, vol. 135, Apr. 1, 1932, pp. 601-616.

13. Flax, Alexander H.: The Influence of Structural Deformation on Airplane Characteristics. J. Aeronaut. Sci., vol. 12, no. 1, Jan. 1945, pp. 94-102.

14. Sandford, Maynard C.; Abel, Irving; and Gray, David L.: Development and Demonstration of a Flutter-Suppression System Using Active Controls. NASA TR R-450, 1975.

TABLE I.- MEASURED AND CALCULATED NATURAL VIBRATION MODE FREQUENCIES

Λ, deg	Measured			Calculated		
	f_1, Hz	f_2, Hz	f_3, Hz	f_1, Hz	f_2, Hz	f_3, Hz
Aspect ratio 4.0						
0	7.1	31.6	44.2	7.5	32.2	46.5
-15	6.8 [a]7.2 [b]6.7	31.2 35.5 30.5	43.6 48.0 42.8	7.1	31.3	45.3
-30	5.7	27.8	39.8	6.0	28.7	41.4
Aspect ratio 8.0						
0	7.0	43.8	59.8	7.4	46.3	59.8
-7.5	6.9	42.8	57.2	7.3	45.5	60.0
-15	6.6	41.2	56.4	7.0	43.2	60.4
-30	5.5	33.4	57.4	5.8	35.3	60.7

[a]Model with 64A010 airfoil contour.
[b]Model with supercritical airfoil contour.

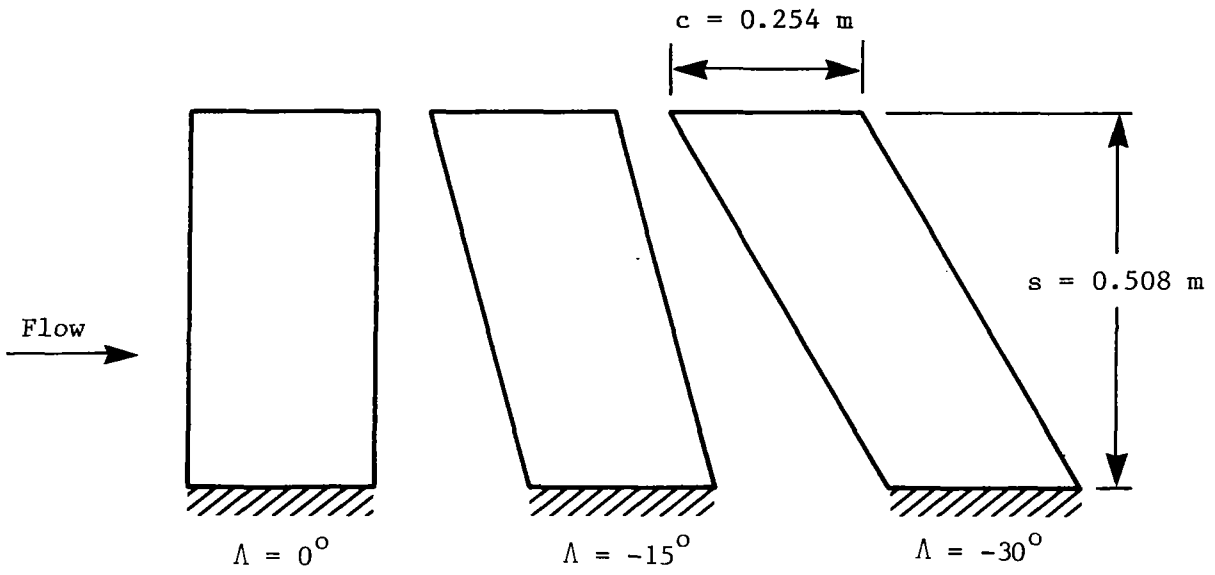

(a) Aspect ratio 4.0.

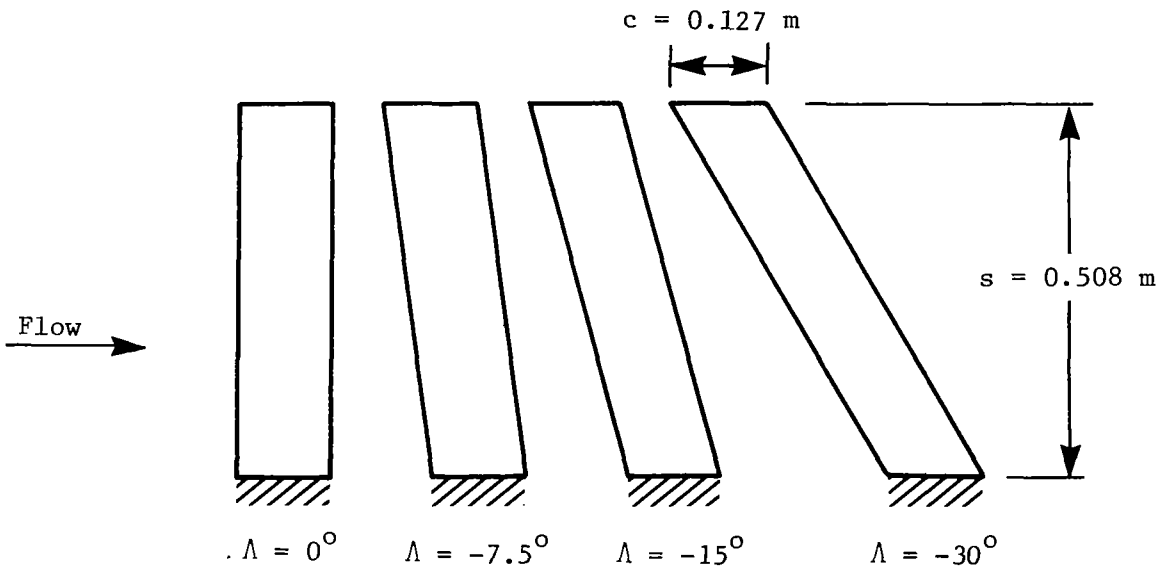

(b) Aspect ratio 8.0.

Figure 1.- Planform geometry of the experimental models.

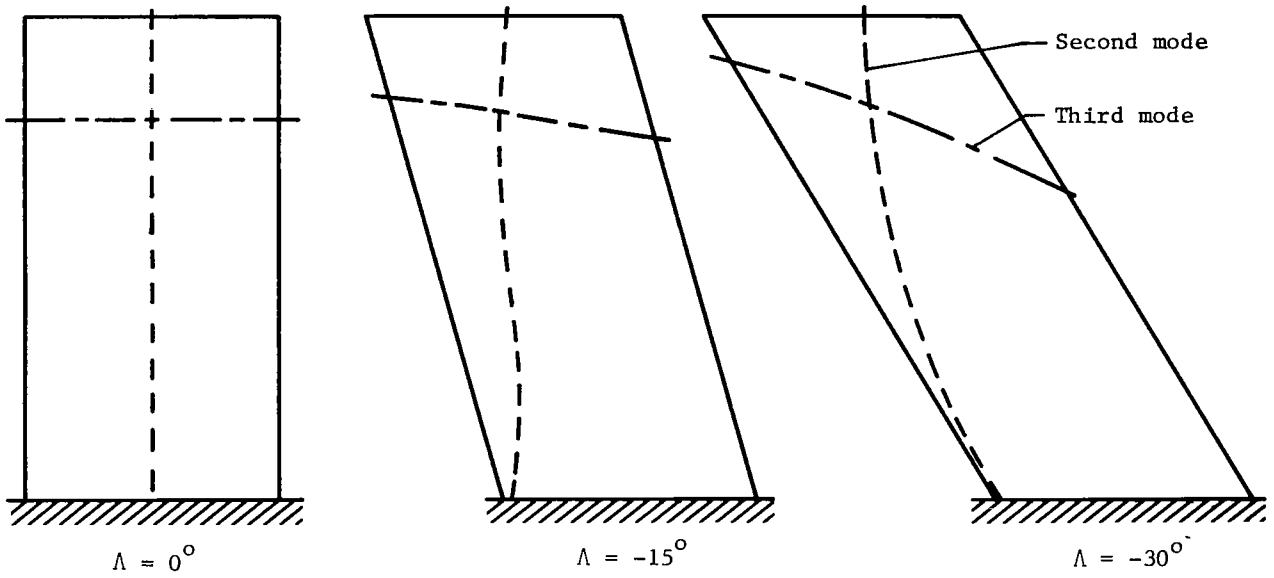

(a) Aspect-ratio-4.0 models.

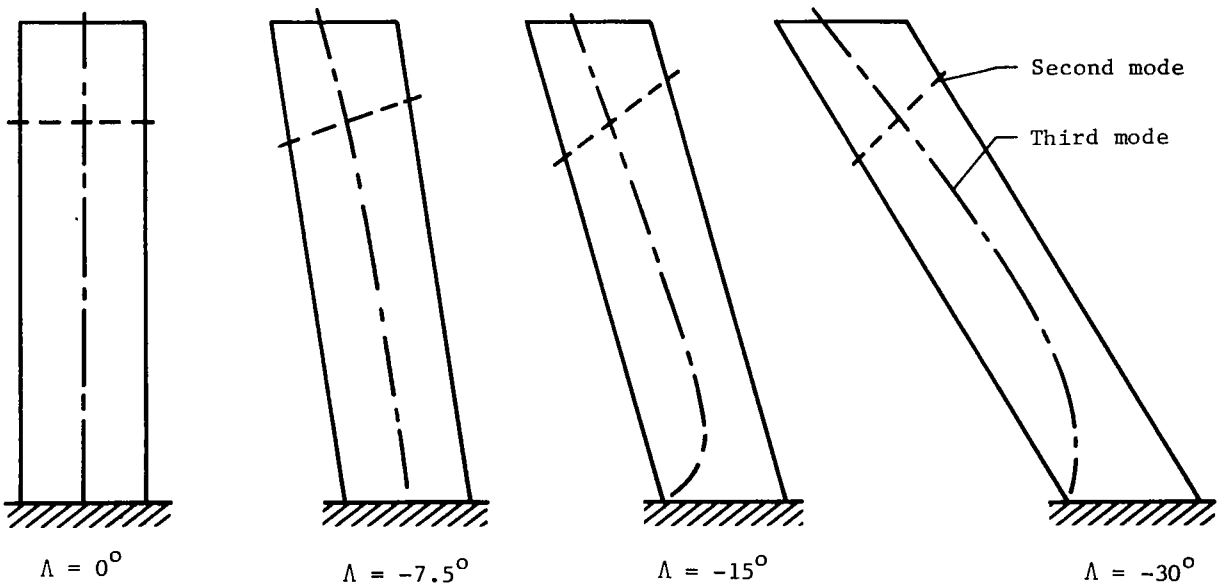

(b) Aspect-ratio-8.0 models.

Figure 2.- Calculated node lines for aspect-ratio-4.0 and aspect-ratio-8.0 models. (Node lines for first mode are along the cantilever root.)

L-78-1969

Figure 3.- Typical model mounted on support with splitter plate installed.

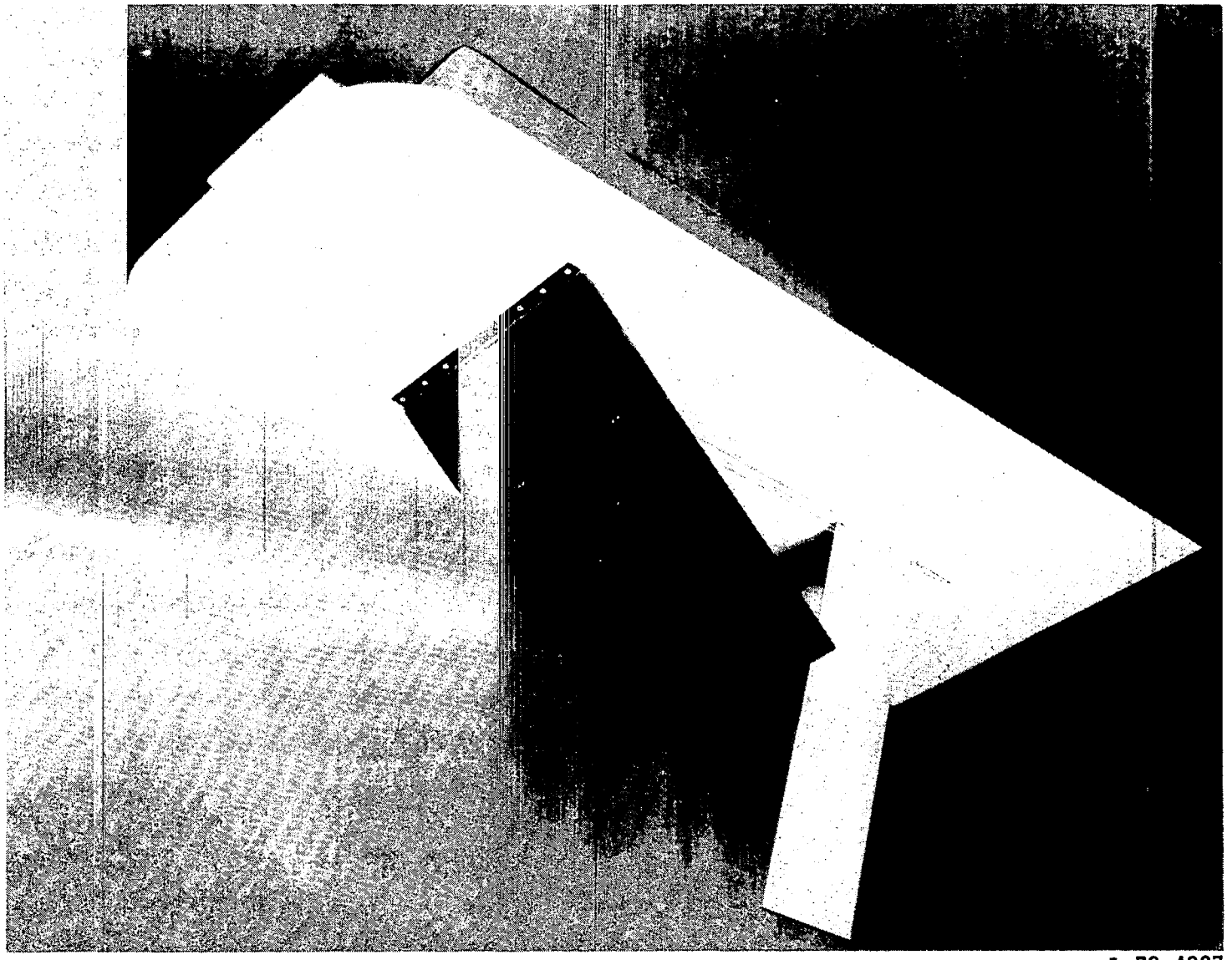

L-78-4287

Figure 4.- Flow-diverter device in extended position for stopping divergence.

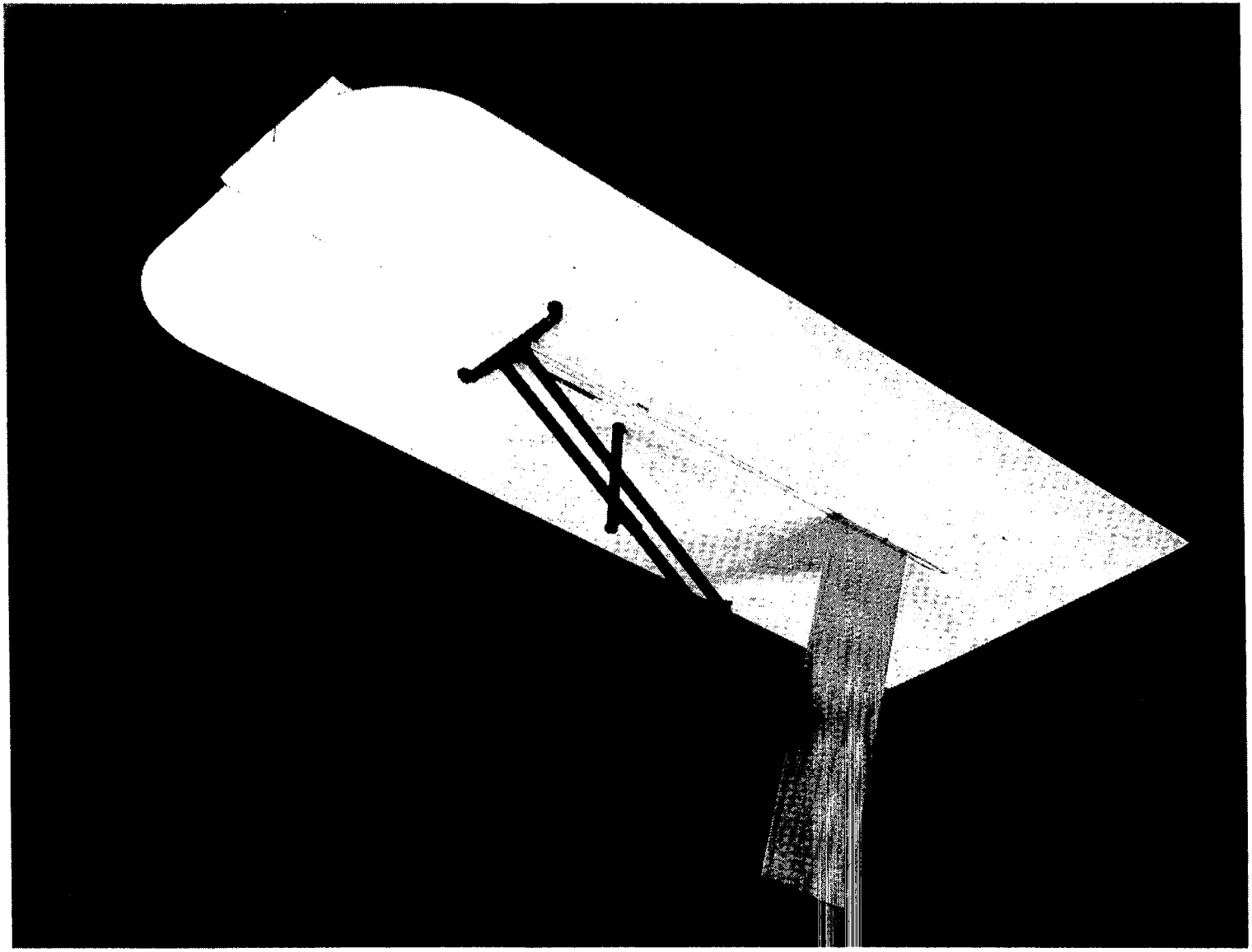

L-78-4291

Figure 5.- Model-constrainer device in extended position for stopping divergence.

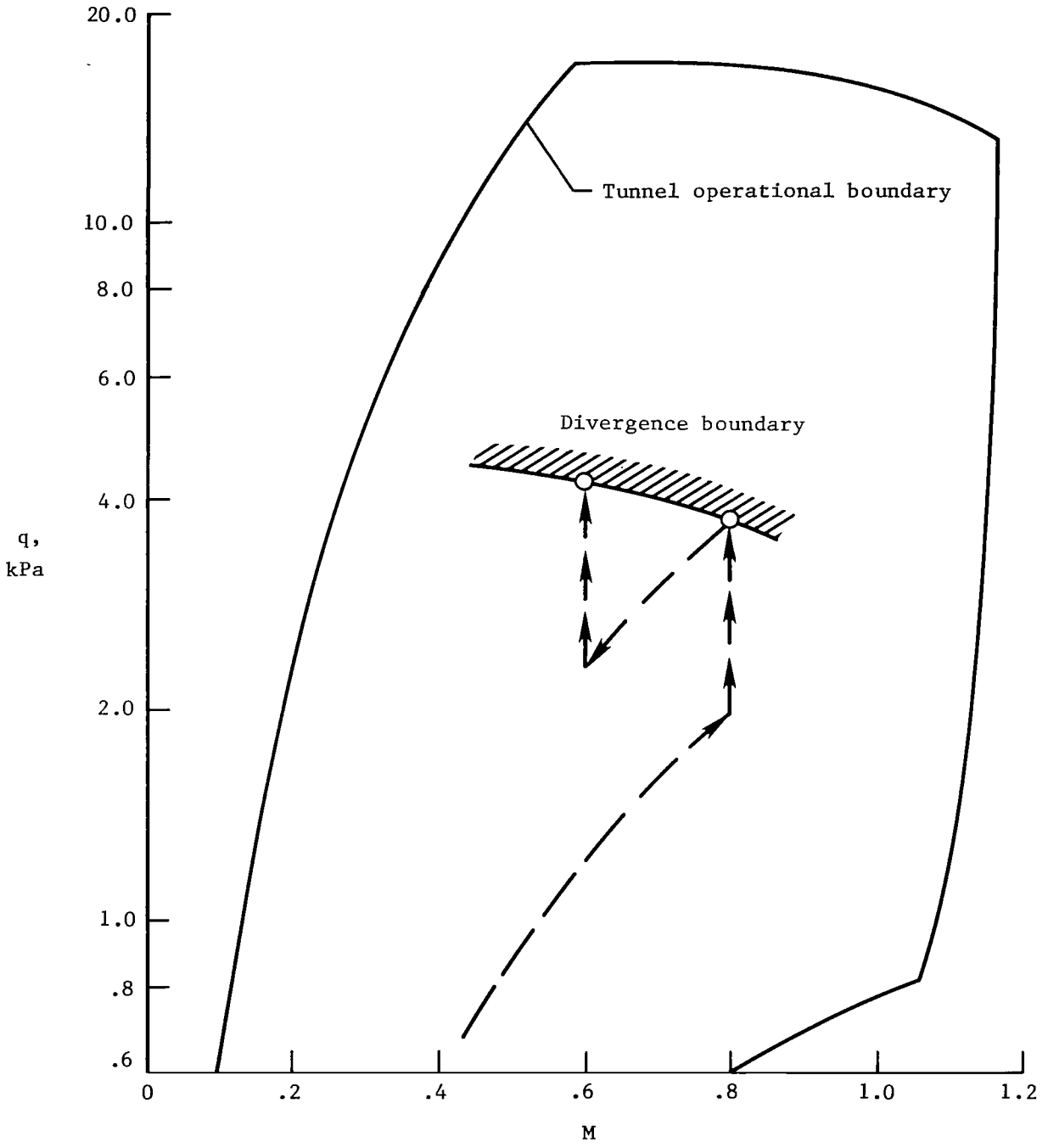

Figure 6.- Test procedure for operation in Freon 12 in Langley Transonic Dynamics Tunnel.

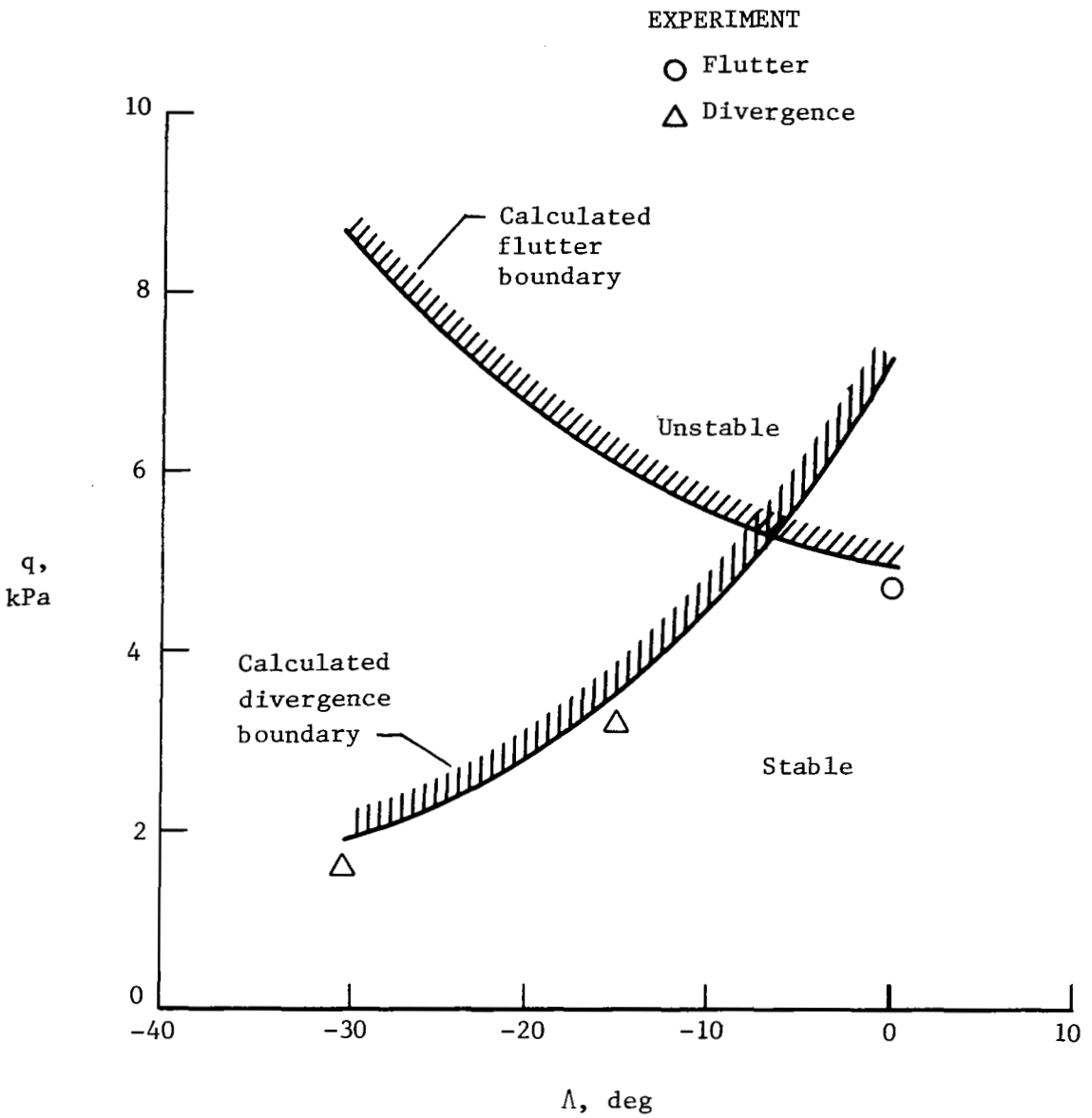

Figure 7.- Experimental instabilities (M < 0.3) for aspect-ratio-4.0 wings compared with calculated boundaries.

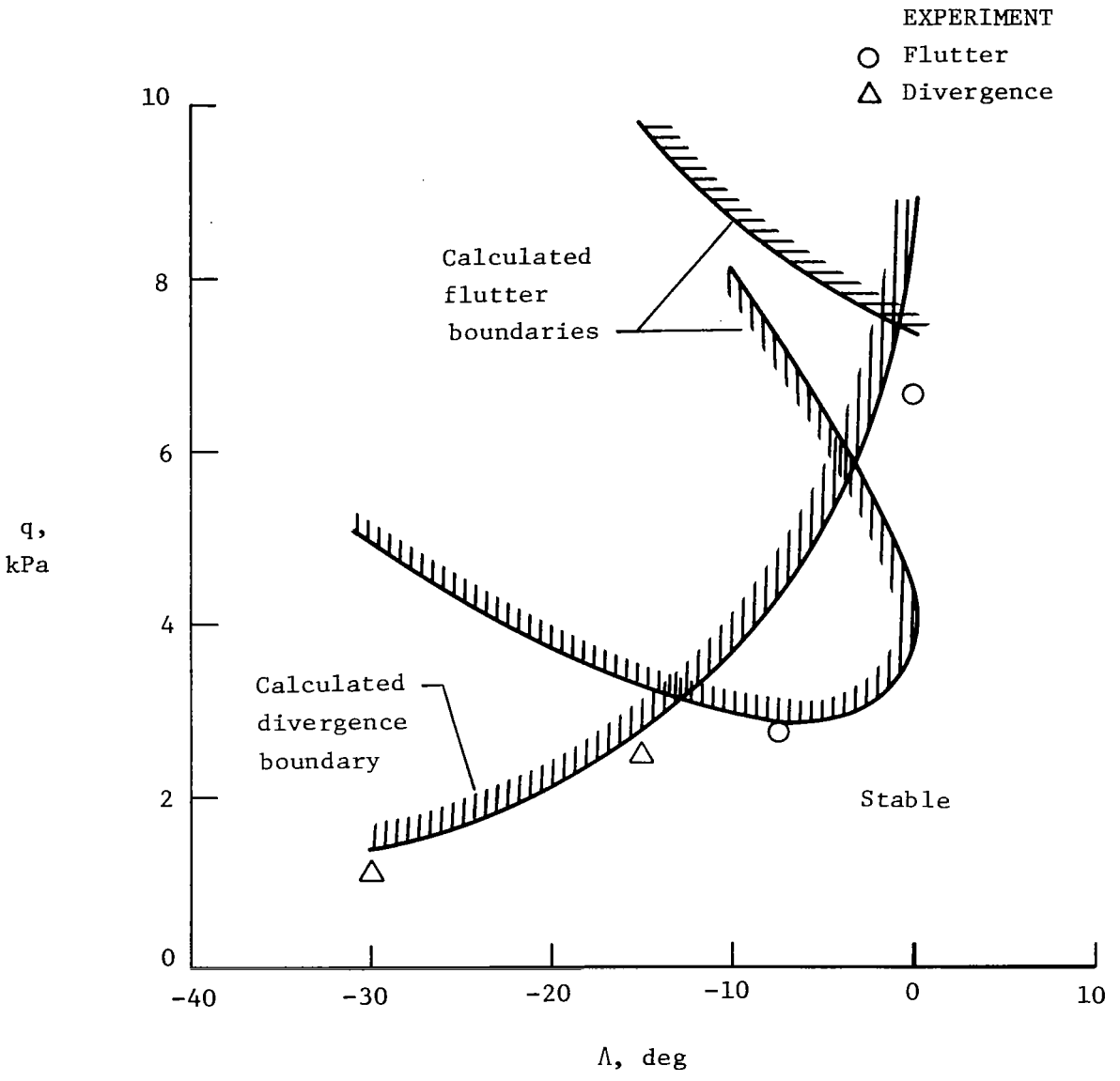

Figure 8.- Experimental instabilities (M < 0.3) for aspect-ratio-8.0 wings compared with calculated boundaries.

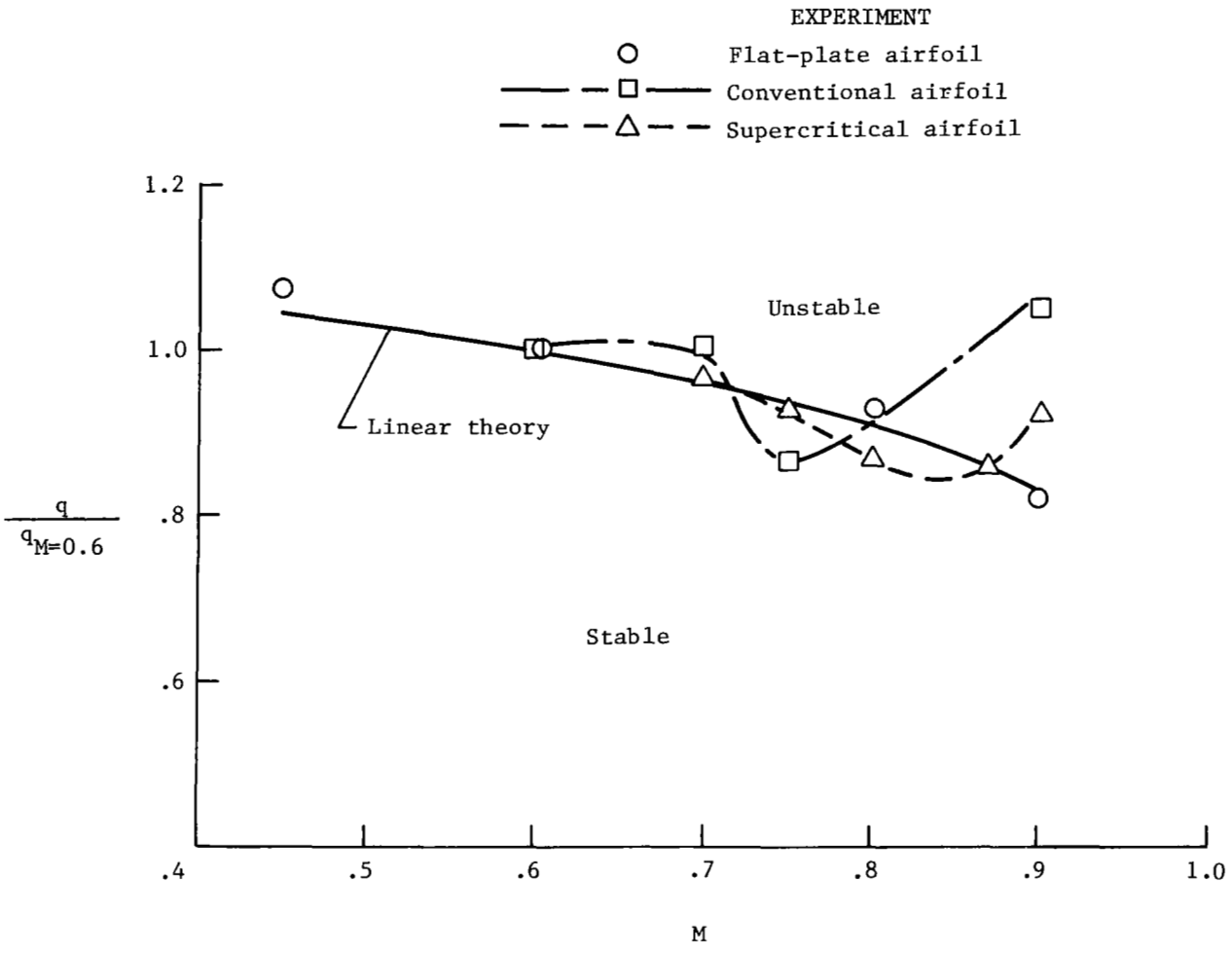

Figure 9.- Comparison of divergence boundaries for flat-plate, conventional, and supercritical airfoil models. $\mathcal{R}$ = 4.0; Λ = -15°.

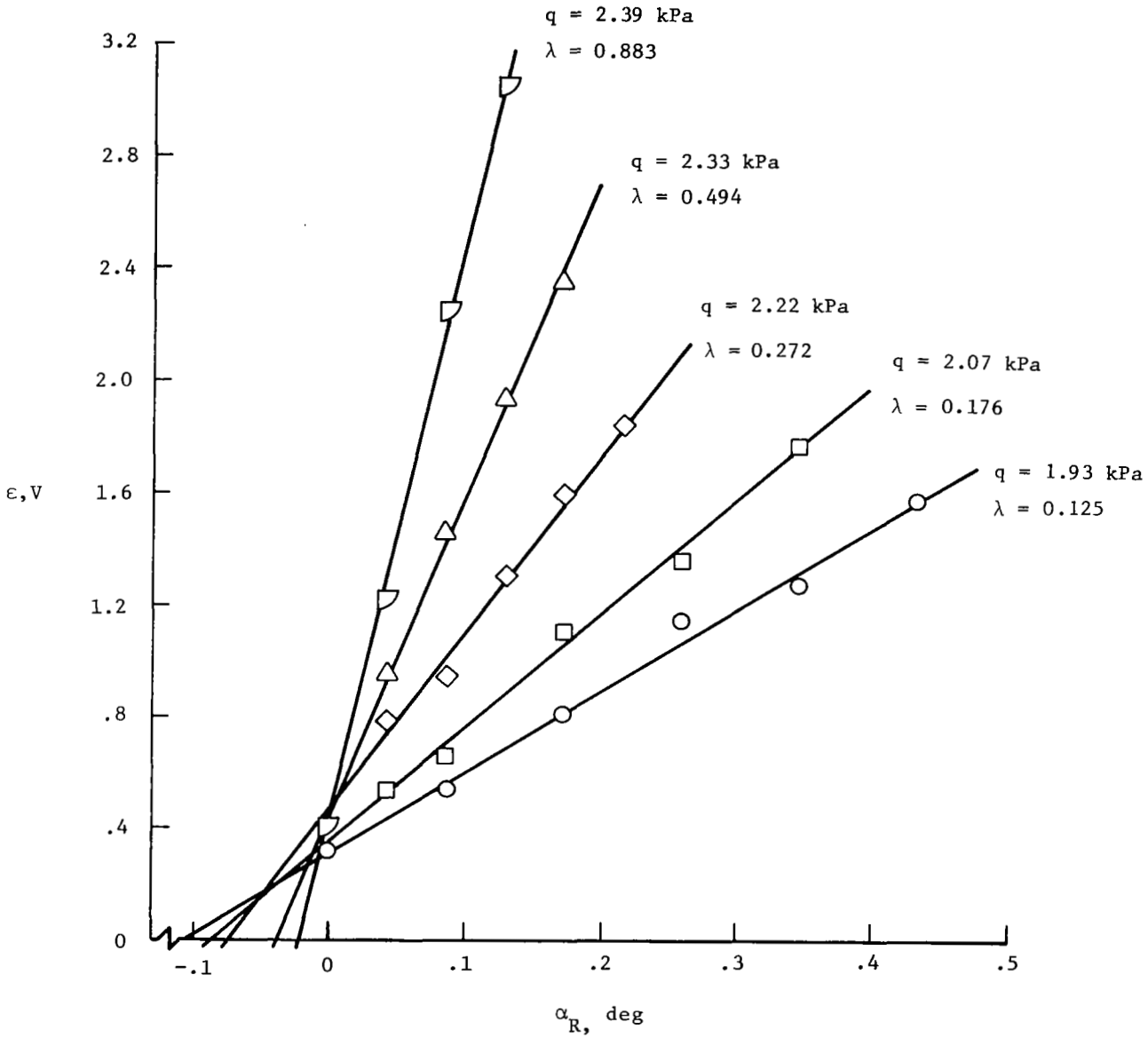

Figure 10.- Basic data for subcritical response divergence prediction techniques. $\mathcal{R}$ = 4.0; Λ = -15°; M = 0.8.

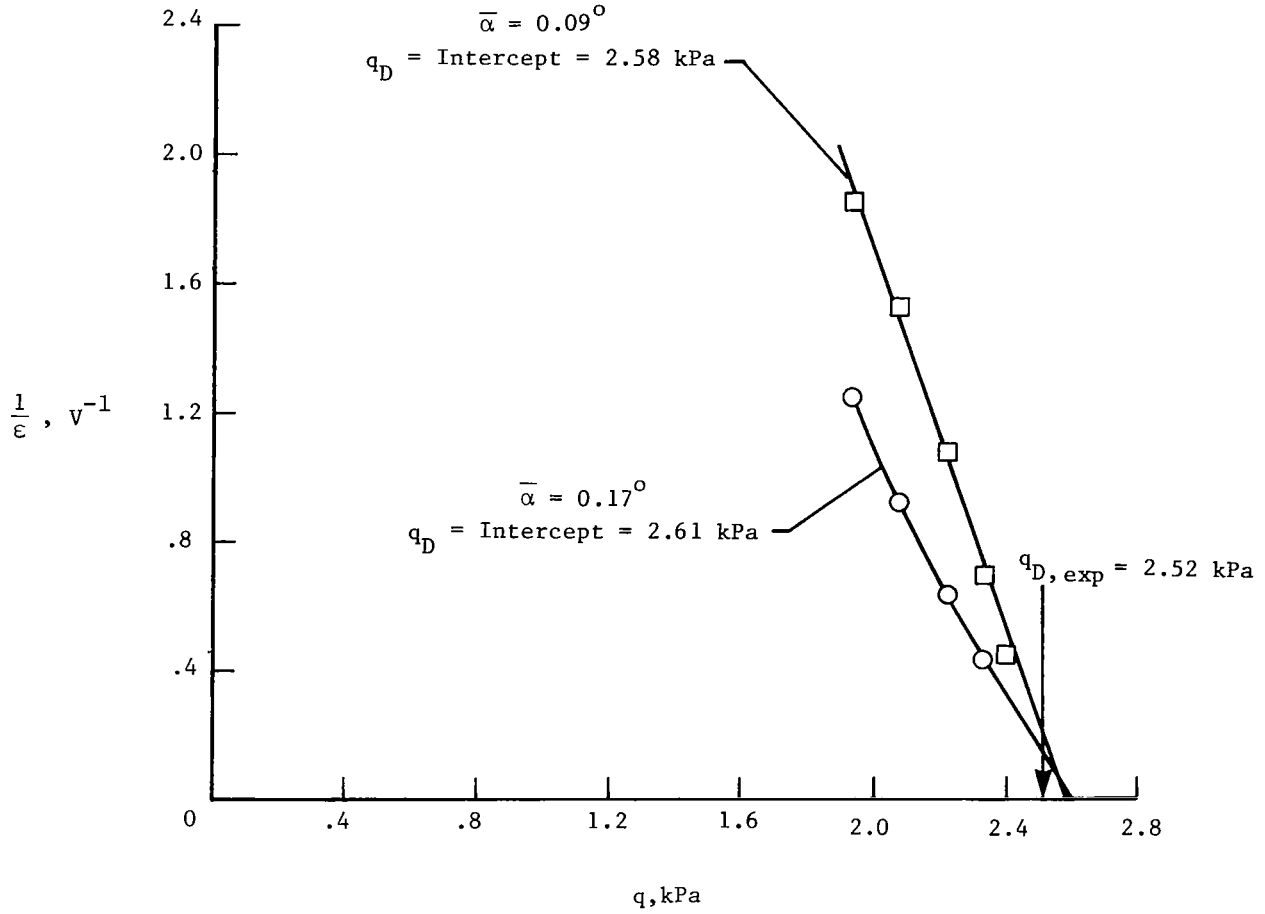

Figure 11.- Static inverse mean strain method for predicting divergence.

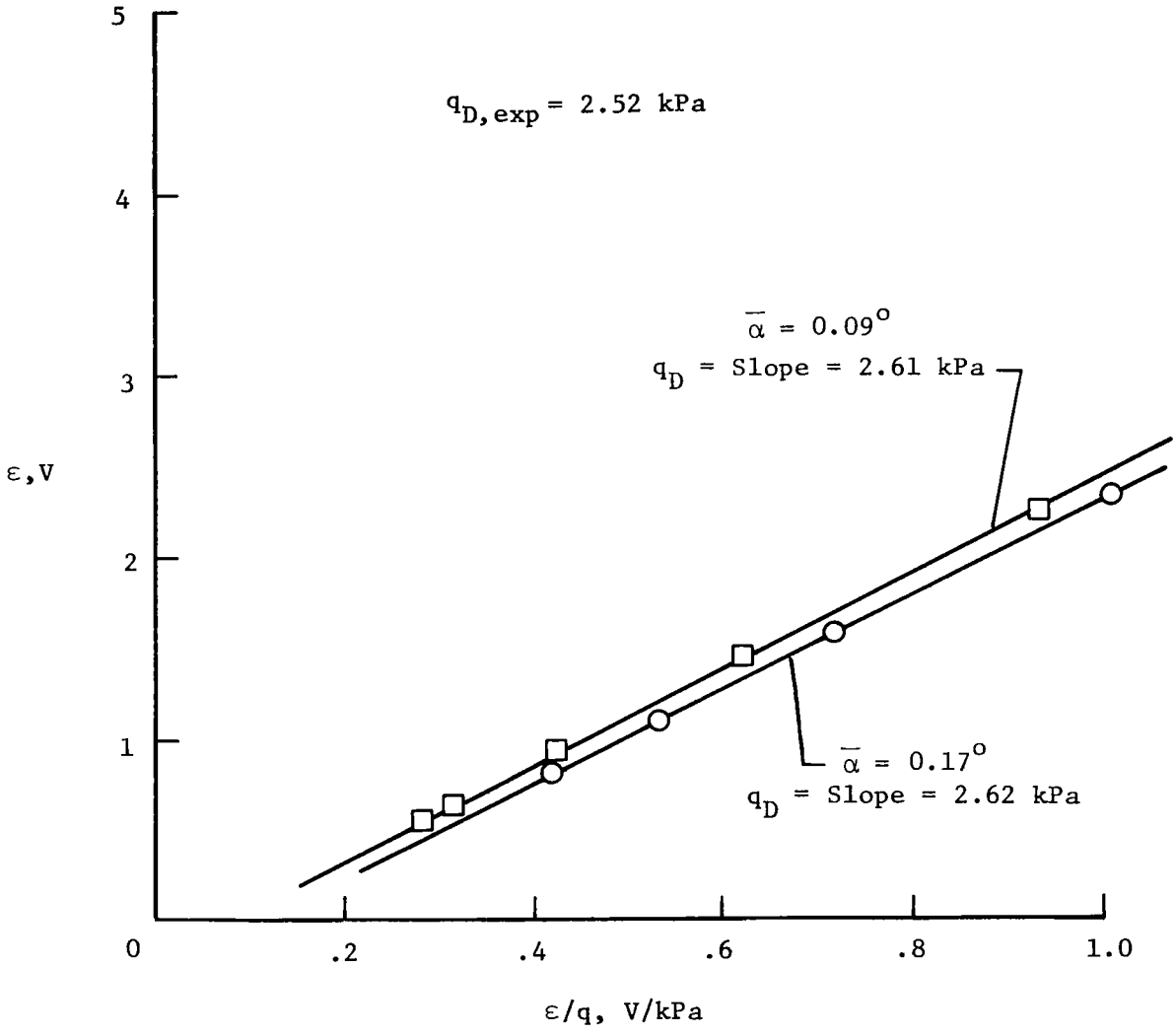

Figure 12.- Static Southwell method for predicting divergence.

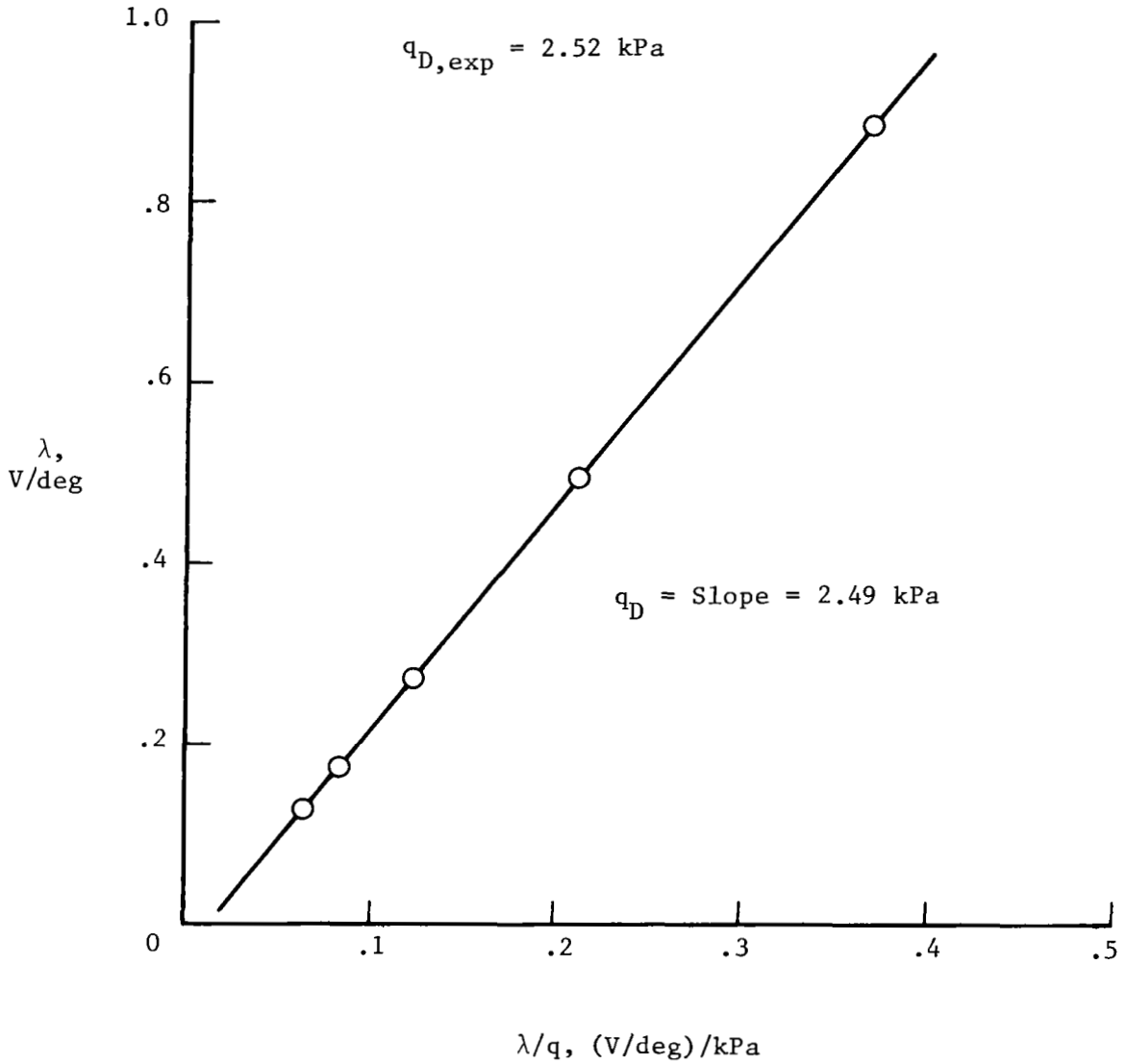

Figure 13.- Improved static Southwell method for predicting divergence.

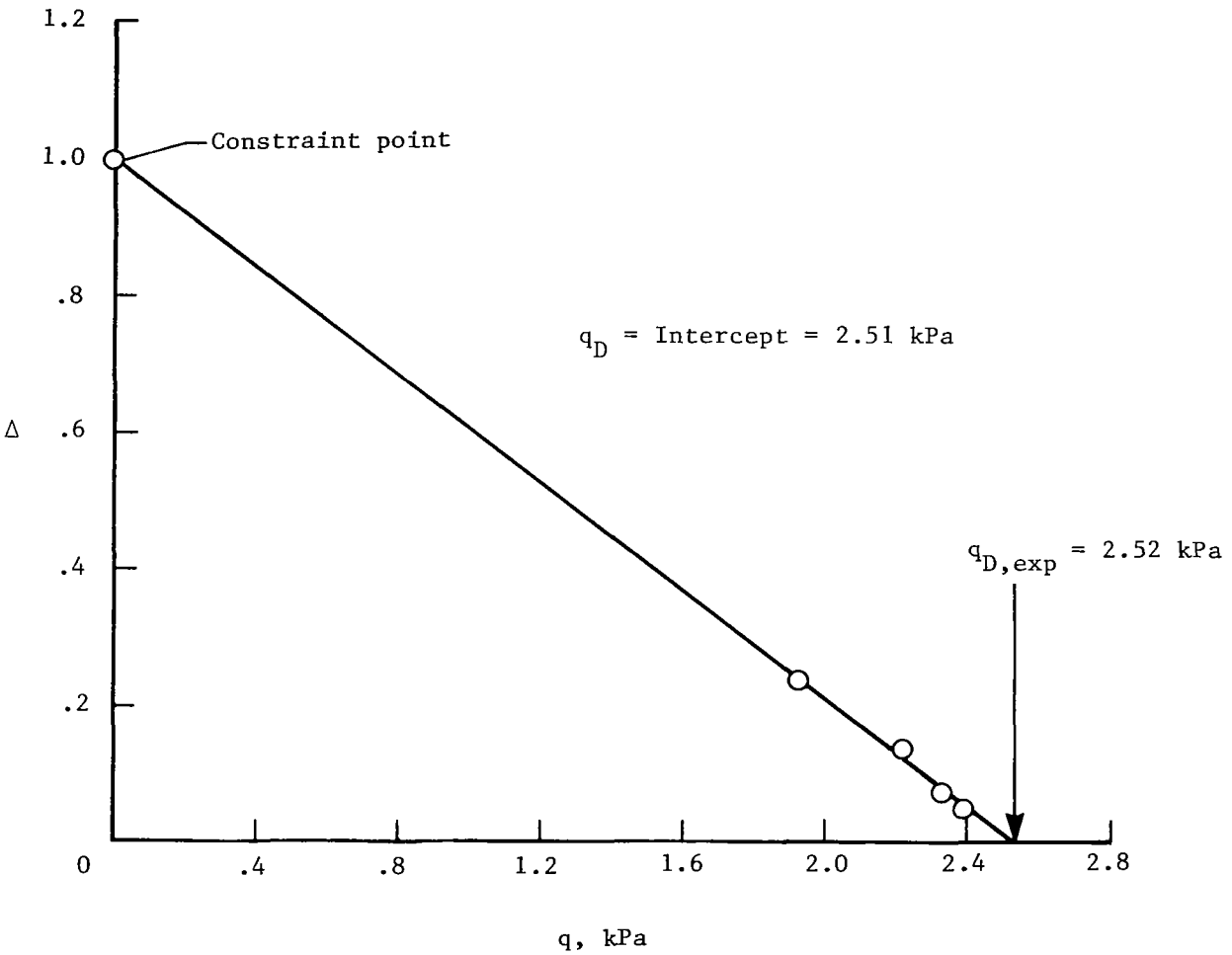

Figure 14.- Static divergence index method for predicting divergence.

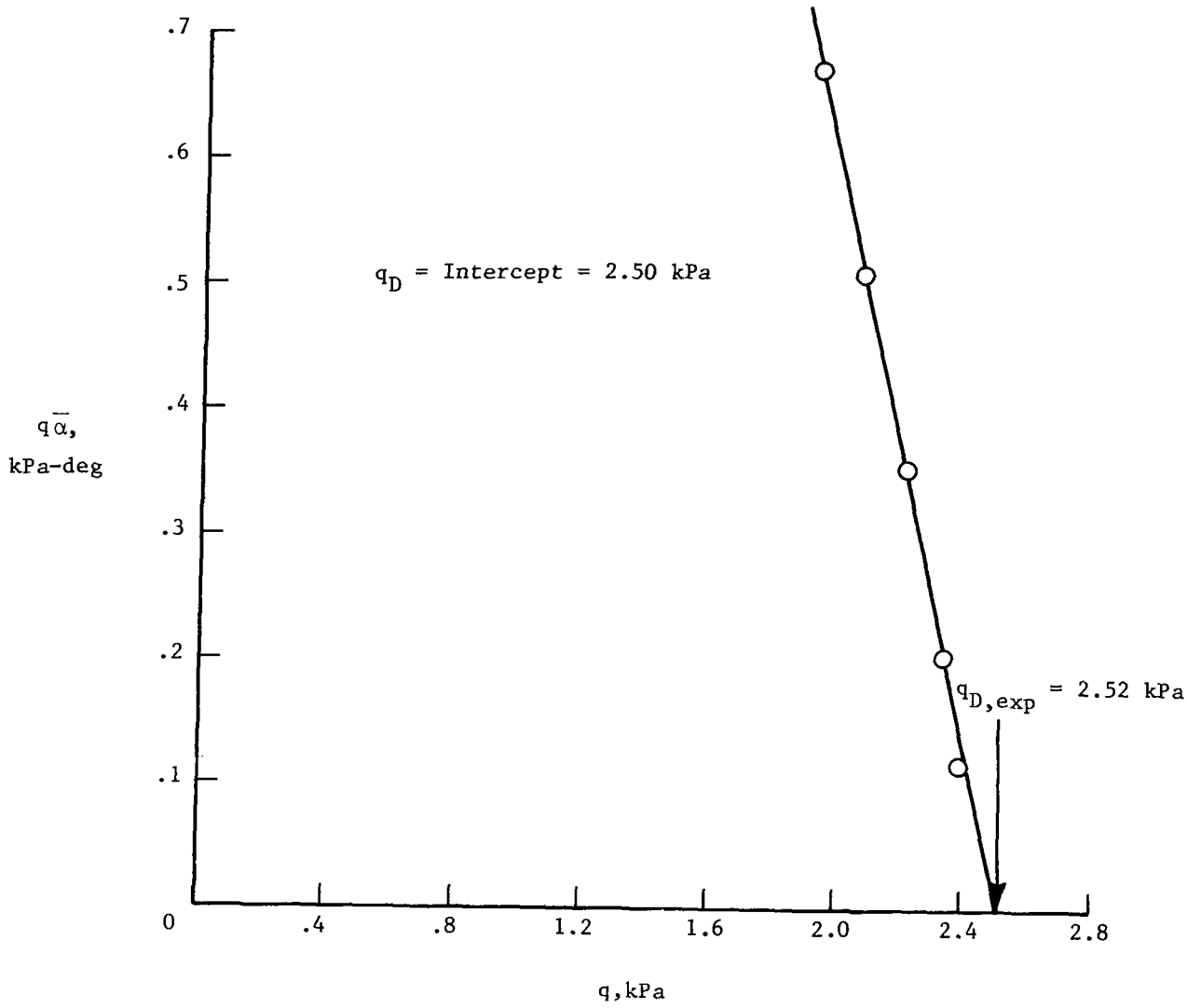

Figure 15.- Static constant-load method for prediction of divergence.

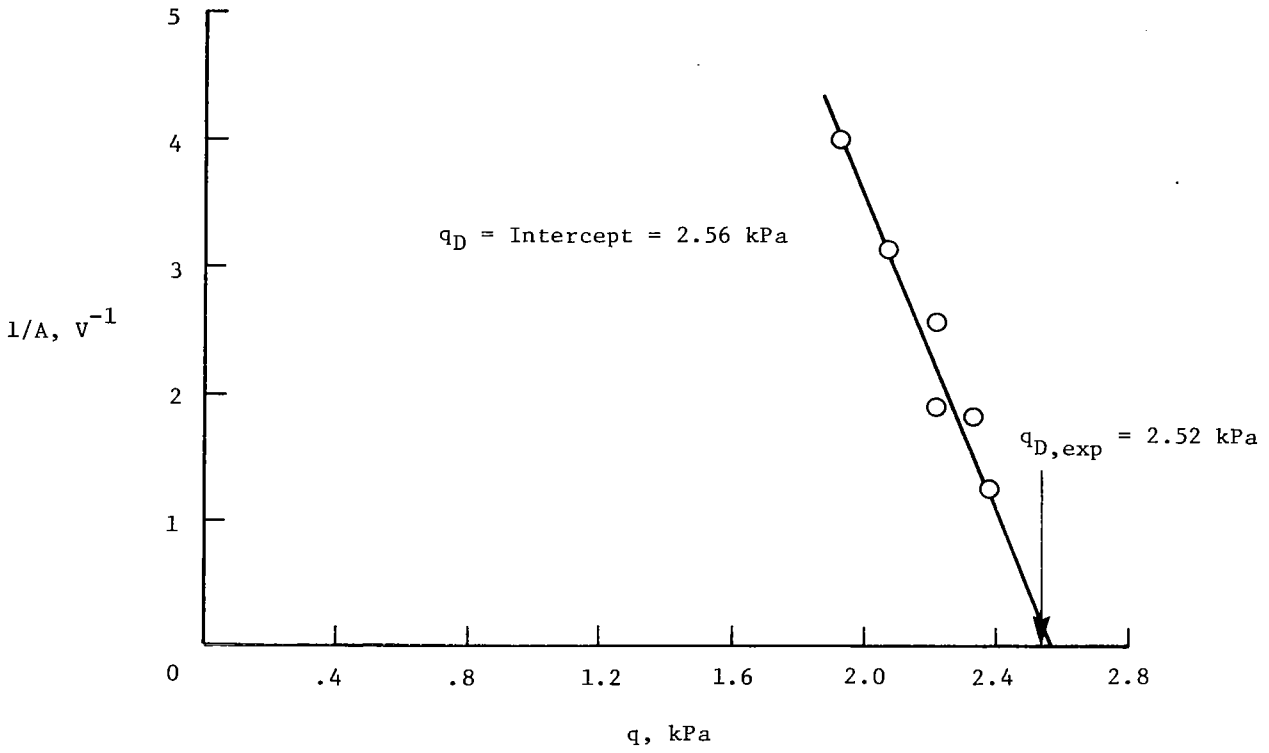

Figure 16.- Dynamic inverse peak amplitude method for predicting divergence.

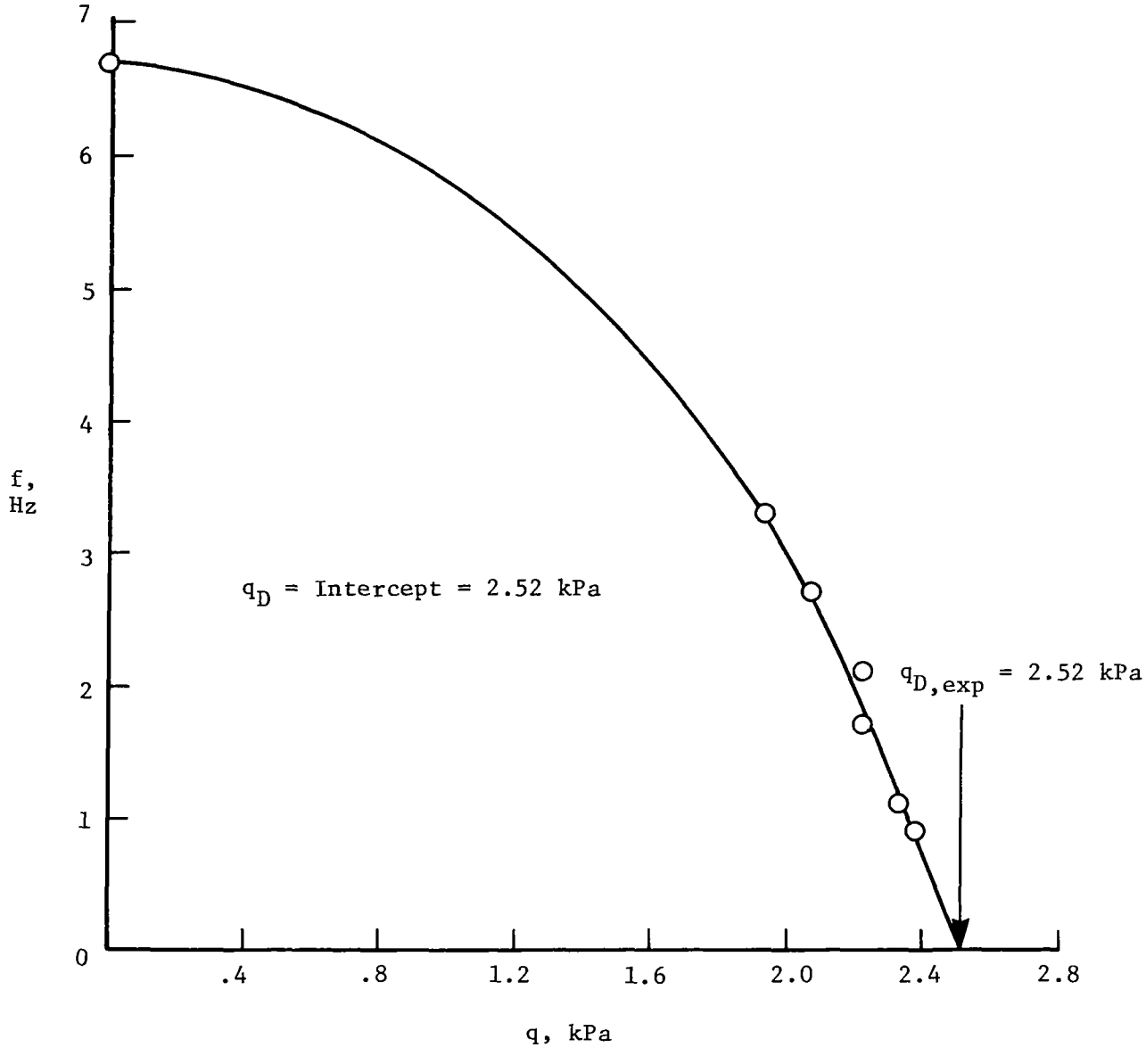

Figure 17.- Dynamic frequency method for predicting divergence.

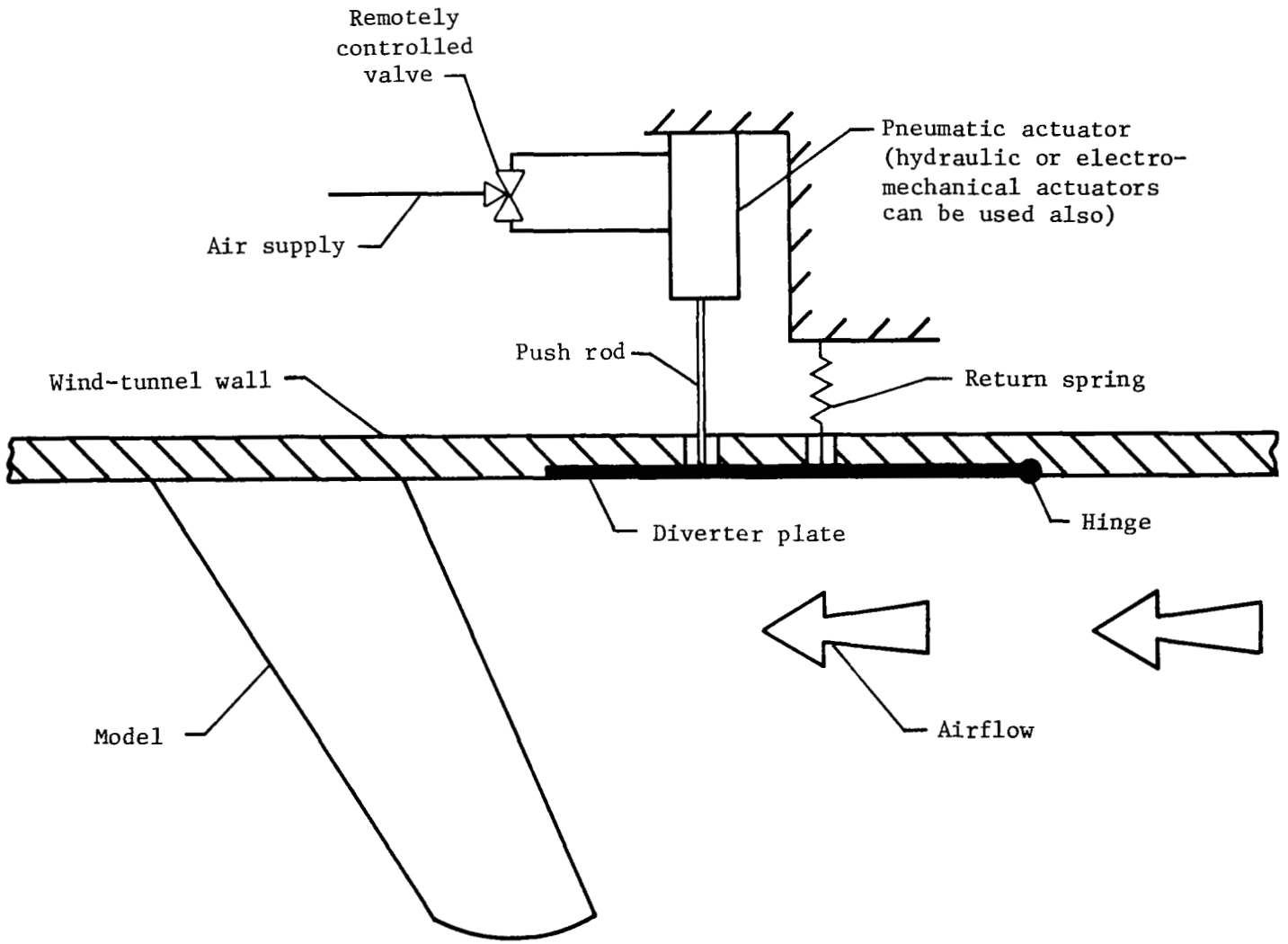

Figure 18.- Flow-diverter device with diverter plate in retracted position.

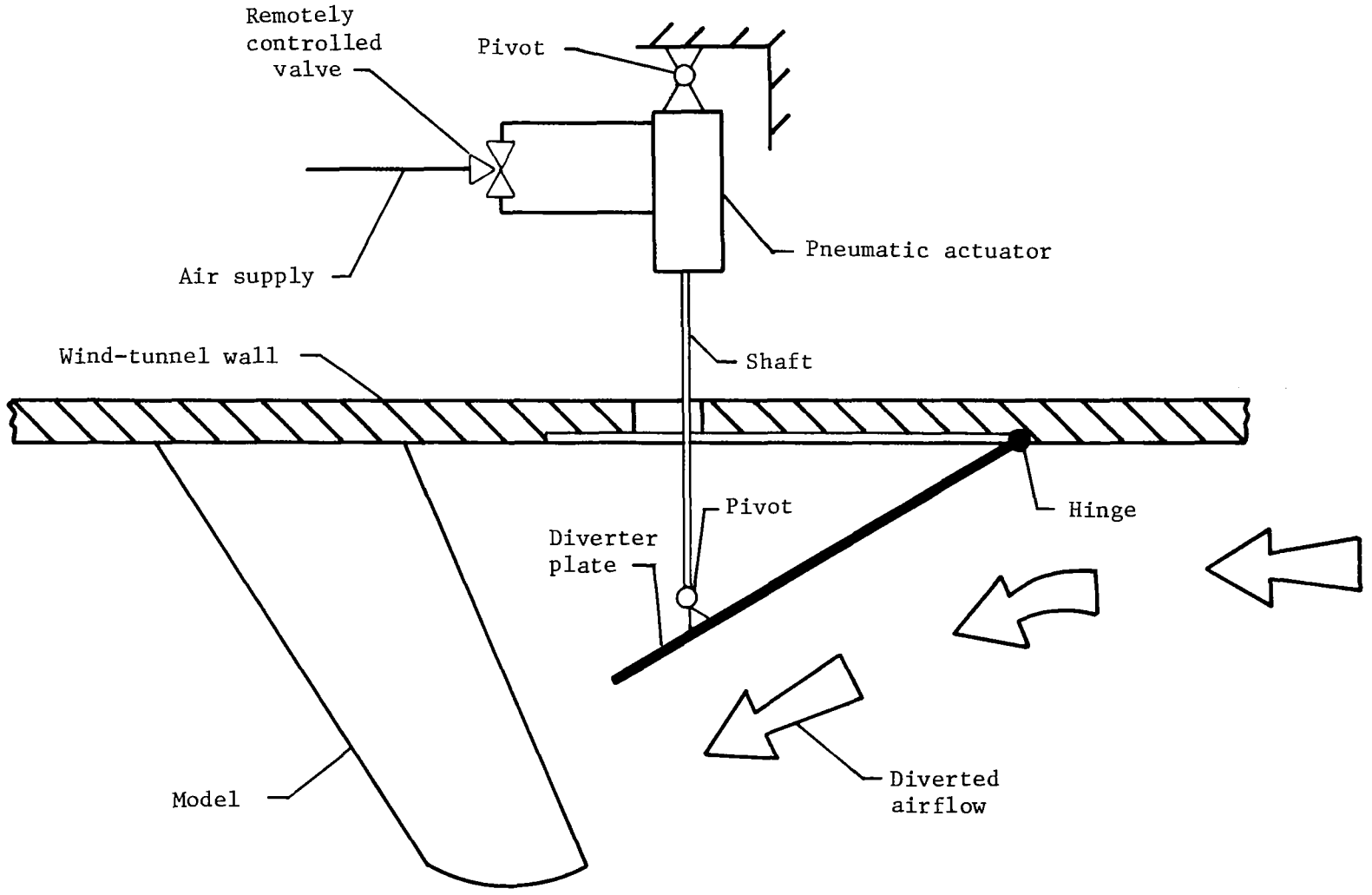

Figure 19.- Flow-diverter device with diverter plate in extended position to stop divergence.

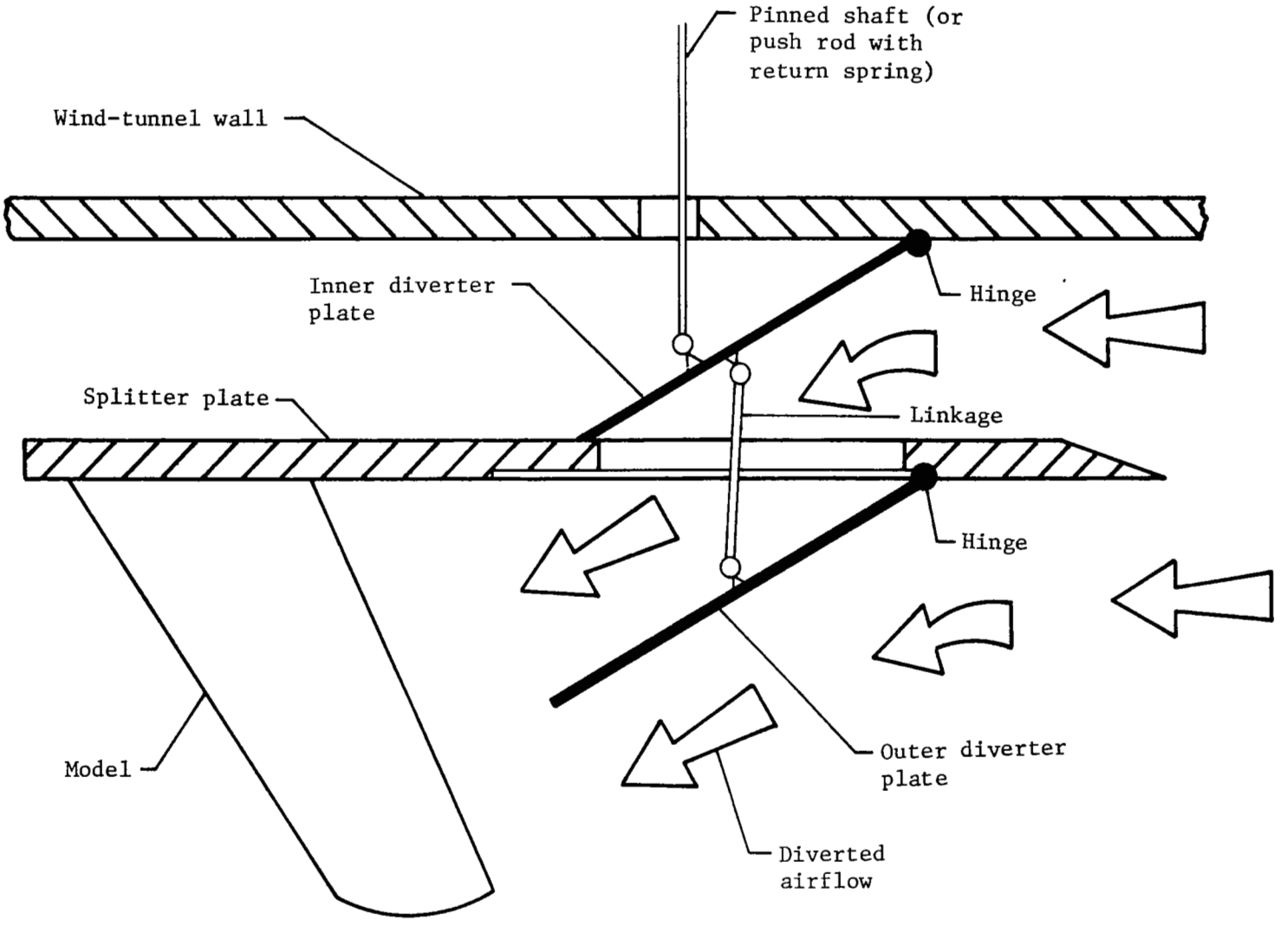

Figure 20.- Flow-diverter device with additional plate to divert boundary-layer air.

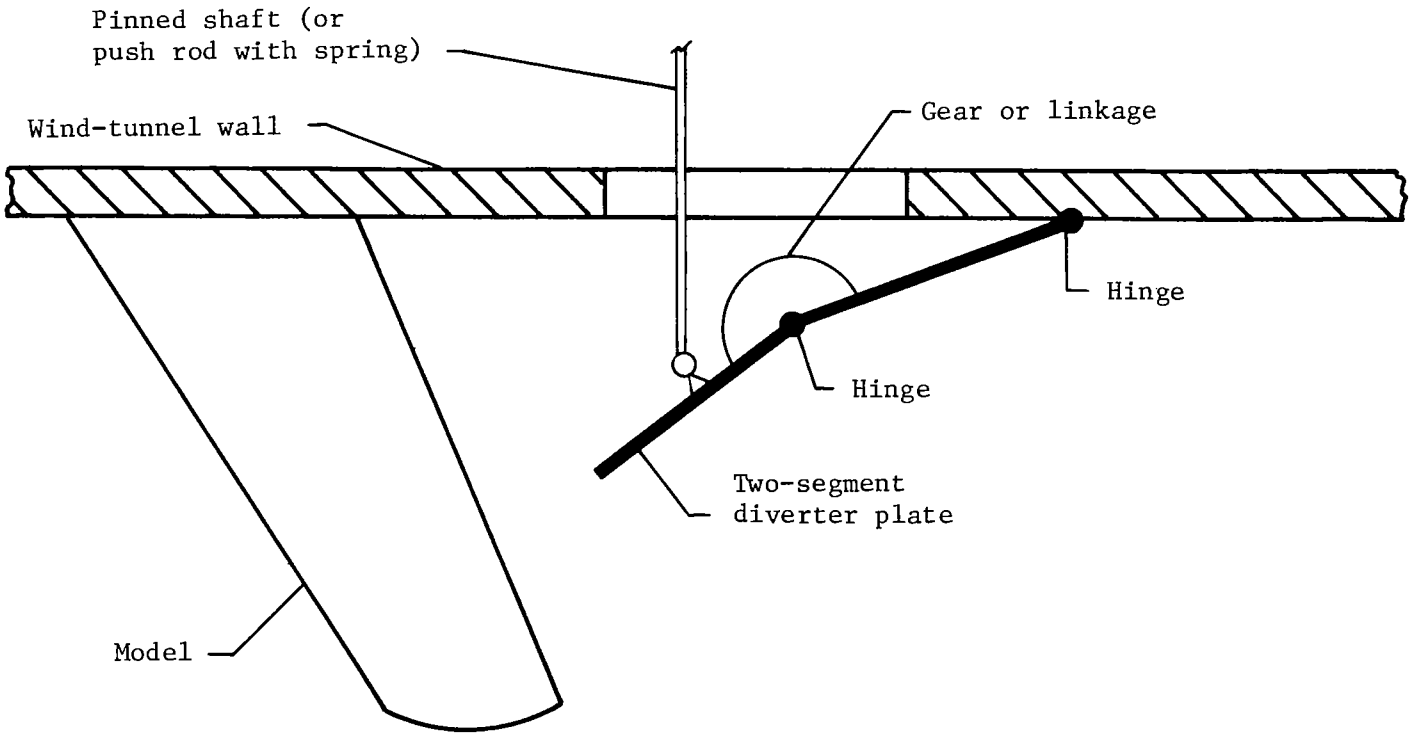

Figure 21.- Flow-diverter device with segmented diverter plate.

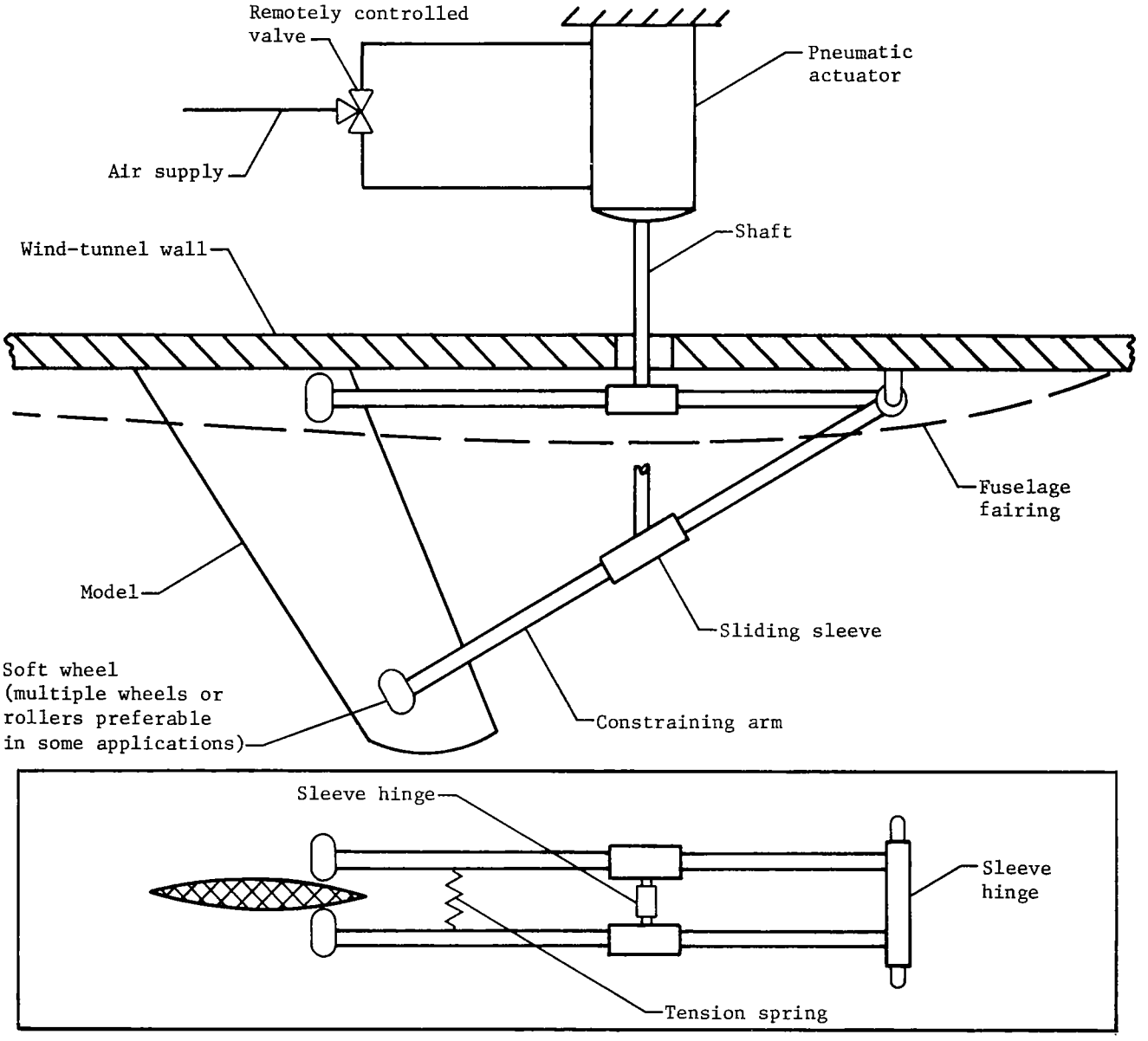

Figure 22.- Model-constrainer device for stopping divergence in retracted and extended positions.

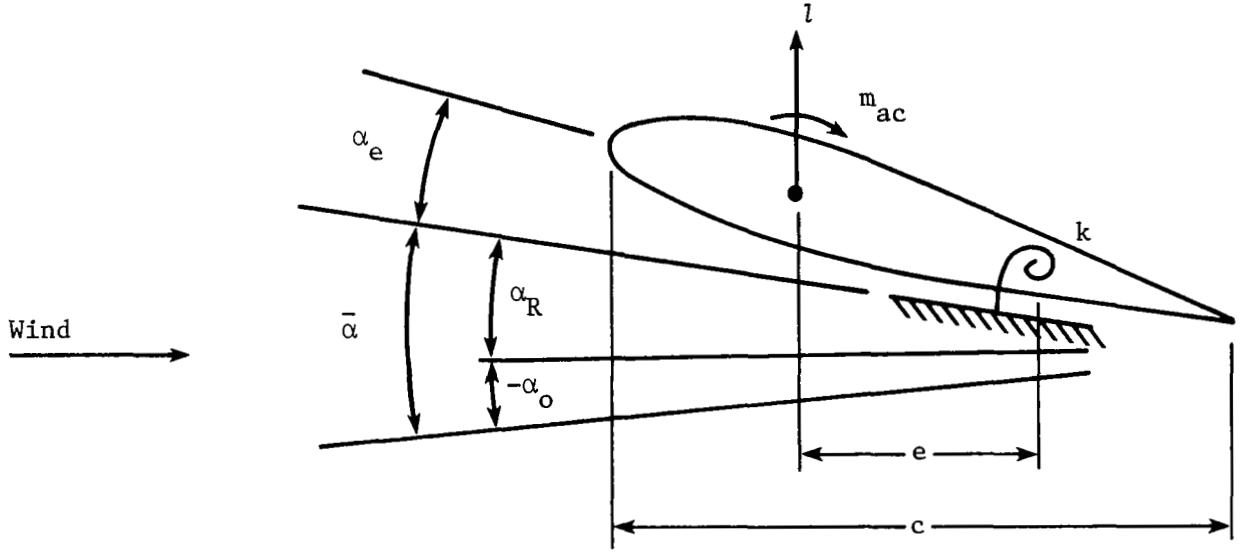

Figure 23.- Idealized aeroelastic system.

1. Report No. NASA TP-1685	2. Government Accession No.	3. Recipient's Catalog No.

4. Title and Subtitle	5. Report Date
WIND-TUNNEL EXPERIMENTS ON DIVERGENCE OF FORWARD-SWEPT WINGS	August 1980
	6. Performing Organization Code
7. Author(s) Rodney H. Ricketts and Robert V. Doggett, Jr.	8. Performing Organization Report No. L-13549
9. Performing Organization Name and Address NASA Langley Research Center Hampton, VA 23665	10. Work Unit No. 505-33-53-01
	11. Contract or Grant No.
12. Sponsoring Agency Name and Address National Aeronautics and Space Administration Washington, DC 20546	13. Type of Report and Period Covered Technical Paper
	14. Sponsoring Agency Code

15. Supplementary Notes

Appendix B by Wilmer H. Reed III, Langley Research Center.

16. Abstract

An experimental study to investigate the aeroelastic behavior of forward-swept wings was conducted in the Langley Transonic Dynamics Tunnel. Seven flat-plate models with varying aspect ratios and wing sweep angles were tested at low speeds in air. Three models having the same planform but different airfoil sections (i.e., flat-plate, conventional and supercritical) were tested at transonic speeds in Freon®12. Linear analyses were performed to provide predictions to compare with the measured aeroelastic instabilities which include both static divergence and flutter. Six subcritical response testing techniques were formulated and evaluated at transonic speeds for accuracy in predicting static divergence. Two "divergence stoppers" were developed and evaluated for use in protecting the model from structural damage during tests.

17. Key Words (Suggested by Author(s))	18. Distribution Statement
Aeroelasticity Divergence Divergence stoppers Forward-swept wings Subcritical response techniques	Unclassified - Unlimited Subject Category 05

19. Security Classif. (of this report)	20. Security Classif. (of this page)	21. No. of Pages	22. Price
Unclassified	Unclassified	46	A03

For sale by the National Technical Information Service, Springfield, Virginia 22161

NASA-Langley, 1980

National Aeronautics and
Space Administration

Washington, D.C.
20546

Official Business
Penalty for Private Use, $300

THIRD-CLASS BULK RATE

Postage and Fees Paid
National Aeronautics and
Space Administration
NASA-451

1 1 1U,A, 070880 S00903DS
DEPT OF THE AIR FORCE
AF WEAPONS LABORATORY
ATTN: TECHNICAL LIBRARY (SUL)
KIRTLAND AFB NM 87117

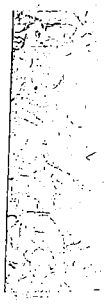

NASA

POSTMASTER: If Undeliverable (Section 158 Postal Manual) Do Not Return